INSTITUTE FOR FUSION STUDIES

DOE/ET-53088-568 IFSR #568

Electron-Temperature-Gradient-Induced Instability in Tokamak Scrape-Off Layers

H.L. BERK, R.H. COHEN,[a] D.D. RYUTOV,[b]
YU.A. TSIDULKO,[b] and X.Q. XU[c]
Institute for Fusion Studies
The University of Texas at Austin
Austin, Texas 78712

[a] *Lawrence Livermore National Lab.*
[b] *Budker Institute for Nuclear Physics, Novosibirsk, Russia*
[c] *Dept. of Electrical Eng., University of California, Berkeley*

August 1992

THE UNIVERSITY OF TEXAS

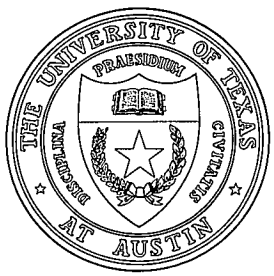

AUSTIN

Electron-Temperature-Gradient-Induced Instability in Tokamak Scrape-Off Layers

H. L. Berk,[1] R. H. Cohen,[2] D. D. Ryutov,[3] Yu. A. Tsidulko,[3] and X. Q. Xu[4]

[1] Institute for Fusion Studies, University of Texas at Austin, Austin, TX 78712

[2] Lawrence Livermore National Laboratory, Livermore, CA 94550

[3] Budker Institute for Nuclear Physics, Novosibirsk, Russia

[4] Department of Electrical Engineering, University of California, Berkeley, CA 94720

Abstract

An electron temperature instability driven by the Kunkel-Guillory sheath impedance, has been applied to the scrape-off layer of tokamaks. The formalism has been generalized to more fully account for parallel wavelength dynamics, to differentiate between electromagnetic and electrostatic perturbations and to account for particle recycling effects. It is conjectured that this conducting wall instability leads to edge fluctuations in tokamaks that produce scrape-off widths of many ion Larmor radii $\gtrsim 10$. The predicted instability characteristics correlate somewhat with DIII-D edge fluctuation data, and the scrape-off layer width in the DIII-D experiment agrees with theoretical estimates that can be derived from mixing length theory.

I. Introduction

Recent theoretical work [1,2] has demonstrated that a vociferous flute instability, induced by electron temperature gradients, is possible for plasmas on open field lines in contact with conducting end-plates. The original work, which is an extension of a plasma model originally discussed by Kadomtsev [3], was oriented toward mirror contained plasmas. However, the basic mechanism causing instability is quite general and there is an obvious application to scrape-off layers in toroidal systems. The purpose of this study is to assess the implications of this instability for toroidal scrape-off layers (in particular tokamaks). We show that, for typical tokamak scrapeoff-layer (SOL) parameters, this instability produces diffusion, comparable in magnitude to Bohm, that should give rise to a temperature SOL width of order 1–2 centimeters (tens of ion gyroradii) even when plasma-particles are lost in an ion transit time. The predicted widths, typical mode frequencies, and relationships between the fluctuations in potential, temperature and density are compatible with experimental observations. We shall also show that moderate edge beta values change the character of the mode, reducing the growth rate and the wavenumber at the maximum growth rate, but have a much weaker effect on the real frequency and the mixing-length estimate of the thermal diffusivity. Various sets of the self-consistent scaling parameters will be presented.

Handling of the heat load on the divertor or limiter is considered to be a major issue for future large tokamaks such as the International Thermonuclear Experimental Reactor (ITER) [4]. Because the cross-field transport sets the width of the scrape-off layer and hence plays an major role in determining the heat flux density on the divertor or limiter, understanding of SOL turbulence is important for the design of such machines. It is also possible that the conditions that determine whether vociferous SOL turbulence is present or not, may be playing a role in the L-to-H-mode transition in tokamaks.

Scrape-off-layer turbulence has been the subject of remarkably few papers. Nedospasov [5] described a mechanism involving a temperature-gradient drive via Pfirsch-Schlüter currents and end loss. Nedospasov [5] also considered, and Garbet *et al.* [6] studied in more detail, turbulence driven by curvature and the polarization drift; the end loss was stabilizing as in the pioneering work of Kunkel and Guillory [7]. The instability

under consideration in this paper, that described in Ref. 2, is driven by a cross-field gradient in the difference of the electrostatic potential between the plasma and the end wall in conjunction with end loss and the polarization drift. It may be verified *a posteriori* that, for parameters relevant to present and future large tokamaks, the present mechanism produces the strongest instability.

The gradient of the potential difference arises naturally from the electron-temperature gradient; hence the mode can be viewed (and was, in Refs. 1 and 2) as being induced by electron temperature gradients. While this is a more familiar instability drive, the instability can also be viewed as due to plasma flow with conducting wall-sheath boundary conditions. In the present presentation we show that there is instability even when there is a fixed $\mathbf{E} \times \mathbf{B}$ flow in the plasma, while at the conducting end walls $\mathbf{E} \times \mathbf{B} = 0$. Instability is possible as there is no moving frame of reference where the electric field can be entirely transformed away. The dispersion relation for such a case was first obtained by Kadomtsev [3] , although its unstable structure was not exhibited then.

This paper, in addition to applying the results of Ref. 2 to scrape-off layers, extends the previous analysis. We present here a much more detailed examination of the mechanism of the instability. Here, we start from the low-beta limit of two-fluid electromagnetic equations and retain finite-parallel-wavenumber effects, taking care to describe the transition from an electrostatic to an electromagnetic mode. We also add moderate secondary electron emission and recycling. Furthermore, we begin to account for variations of equilibrium parameters along field lines by allowing the end-loss current to be governed by different densities and temperatures than the mid-plane values used to characterize the bulk of a field line. Additionally, there is a more extensive consideration of the nonlinear state of the mode.

The organization of the paper is as follows. We begin, in Sec. II, with the physical description of the instability. Section III is a derivation of the eigenmode equation. The end-loss (sheath) physics is discussed in Sec. IV, and the dispersion relation is obtained and analyzed in Sec. V. Section V also includes mixing-length diffusivity estimates and discussion of other aspects of the nonlinear (turbulent) state of the mode. Section VI is devoted to estimates of the self-consistent transport which follows from the results of Sec. V,

and Sec. VII applies the results of the preceding sections to the DIII-D [8] experiment and to ITER. Section VIII includes a summary of results and a list of issues requiring further attention.

We note, particularly in connection with Sec. VI, that we are using the term "scrape-off layer" to refer to the centimeter-or-so wide region of open field lines, immediately surrounding the closed-field-line core, which is directly energized by power flowing out from the core. Further out, this SOL typically fades into a longer-scale-length, low-density, low-temperature region which is better described as the halo region. While the instability under discussion can exist in the halo, that region is dominated by local sources and sinks of particles and energy (and is thus largely decoupled energetically from the core).

In this discussion we shall assume that eikonal approximation in the direction perpendicular to the magnetic field applies. The response parallel to the magnetic field is obtained from a drift-wave expansion ($\omega/\omega_{ci} \sim \epsilon^2$, $k_\parallel/k_\perp \sim v_d/v_t \sim \epsilon$; v_d = drift velocity; v_t = thermal speed) of the two-fluid Braginskii [9] equations. In the limit $k_\perp^2 c^2/\omega_{pe}^2 \ll 1$ (typically satisfied in tokamak scrape-off layers), the response is identical to that obtained from reduced ideal MHD equations if we neglect equilibrium parallel electric fields. In particular, the response is flute-like when the axial scale-length L satisfies $L < v_A/[\omega(\omega+\omega_i^*)]^{1/2}$ [here $v_A = B/(4\pi n_i m_i)^{1/2}$ is the Alfvén speed, n_i the ion density, $Zn_i = n_e \equiv n$, where $n_e \equiv n$ is the electron density, m_i the ion mass, ω the mode frequency, $\omega_i^* = (\mathbf{k}\times\mathbf{b})\cdot\nabla(n_i T_i)/m_i\omega_{ci}n_i$ is the ion diamagnetic frequency, $k_\perp$ the perpendicular wave number, $\mathbf{b}$ the unit vector along the field line, T_i the ion temperature, $\omega_{ci} = ZeB/m_i c$ the ion cyclotron frequency, e is the electron charge, and Z is the atomic number]. We note that in the opposite limit $\omega_{pe}^2/k_\perp^2 c^2 \ll 1$, the response is purely electrostatic. The formalism applies to multiple ion species provided that we interpret m_i, Z and ω_i^* as mean quantities, $m_i = \sum m_j n_j / \sum n_j$, $Z = \sum Z_j n_j / \sum n_j$ and $\omega_i^* = \sum \omega_j^* n_j / \sum n_j$, where the sum runs over all ion species j.

II. Physical Description of Instability

In an open-ended plasma where the electron temperature varies in the radial direction, a radial electric field is characteristically present because an ambipolar potential is needed to regulate the electron endloss to maintain quasineutrality. As the ambipolar potential,

Φ, is proportional to the electron temperature T_e, with typically $\Lambda \equiv e\Phi/T_e \sim 4$, the radial electric field is $-\nabla\Phi \approx -\Lambda\nabla T_e$. As we shall see and as is contained in Ref. 10, the prime cause of the instability is associated with the plasma flow speed, $\mathbf{v}_E \approx -c\nabla\Phi\times\mathbf{B}/B^2$ where we neglect the ion diamagnetic flow in this section. As $\nabla\Phi$ and ∇T are closely coupled together, the instability was originally interpreted as an electron temperature instability, a designation we shall keep in this work. However, one should remember that other transport mechanisms can cause $\nabla\Phi$ to be present even with $\nabla T_e = 0$. For example, if there is a spatial gradient in the mean ion mass, the spatial variation of the sonic outflow would cause a potential gradient in the equilibrium.

For a plasma slab model one usually asserts that cross-field flow does not produce instability. An exception is when the plasma is bounded by conducting end plates. We take the magnetic field in the z-direction and the flow in the y-direction. In addition plasma is being lost to the conducting plates (in the x-y plane) due to plasma outflow onto the walls. The usual stability statement follows by observing that if we had an infinite plasma in the z-direction, one could transform away the electric field by choosing a frame of reference moving with the plasma. However, in the present problem, where the conducting plates are equipotentials, the electric field cannot be completely transformed away everywhere.

Now one has to take into account the physics associated with the Debye sheath between the plasma and the conducting walls that maintains a floating potential $\Phi_d(x) = \Lambda T_{ed}(x)/e$ in the plasma with respect to the conducting wall, with the subscript d denoting plasma characteristics in the pre-sheath that is a distance less than an electron mean free path from the wall. For sufficiently high electron collisional frequencies the end current $J_\parallel[\Phi_d(\mathbf{r}_\perp), T_{ed}(\mathbf{r}_\perp), n_{ed}(\mathbf{r}_\perp)]$, through the Debye sheath, is of the form

$$J_\parallel\left[\Phi_d(\mathbf{r}_\perp), T_{ed}(\mathbf{r}_\perp), r_d(\mathbf{r}_\perp)\right] \cong en_{ed}\left[c_s - \frac{(T_{ed}/m_e)^{1/2}}{2\sqrt{\pi}}\exp\left(-\frac{e\Phi_d}{T_{ed}}\right)\right] \qquad (1)$$

where $c_s^2 \simeq (T_e + T_i)/m_i$, $T_{ed}(\mathbf{r}_\perp)$ is the electron temperature on the plasma side of the sheath, at distance less than a mean free path from the wall. In equilibrium the potential $\Phi_d(\mathbf{r}_\perp)$ needs to adjust so that most of the electrons are reflected back into the plasma in order to maintain quasineutrality on a field line. Though there can in practice be current

emerging from a given field line, to a good approximation the equilibrium $J_\parallel$ can be taken to vanish.

Now let us consider a flute perturbation of the equilibrium where $\xi = \boldsymbol{\xi} \cdot \mathrm{e}_x$ is nearly constant along a field line. The potential perturbation produces an incompressible $\mathbf{E} \times \mathbf{B}$ drift motion. The displacement $\boldsymbol{\xi}$ satisfies

$$\frac{d}{dt}\boldsymbol{\xi} = -i\Omega(s)\boldsymbol{\xi} \equiv \tilde{\mathbf{v}} = -c\frac{\nabla\tilde{\phi} \times \mathbf{b}}{B} \approx -\frac{ic\mathbf{k} \times \mathbf{b}\phi}{B} ,$$

where $\Omega(s) = \omega - \omega_E(s)$ and $\omega_E = \mathbf{k} \cdot \mathbf{v}_E(s)$. Here ϕ is the perturbed potential at a fixed (Eulerian) point $\mathbf{r}$, and $\mathbf{k}$ the WKB wave number. To linear order ϕ is related to the Lagrangian perturbed potential by $\phi = \phi_L - \boldsymbol{\xi} \cdot \nabla\Phi$. In the limit $k_\perp^2 c^2/\omega_{pe}^2 \ll 1$ the plasma response is magnetohydrodynamic, so that the flux may be viewed as moving with the $\mathbf{E} \times \mathbf{B}$ motion. To a first approximation, the temperatures and density also convect with the $\mathbf{E} \times \mathbf{B}$ motion. If we further assume that transport processes and sources convect with the field line perturbation, then virtually nothing changes in the determination of local plasma profiles for density, temperatures and pressure, along the moving flux tube. (In particular, in this approximation there is no perturbation of the parallel heat conduction.) Hence the Lagrangian perturbations of the density and temperatures vanish. The exception is the plasma potential $\tilde{\phi}_L$. The Lagrangian potential perturbation, $\tilde{\phi}_L$, as given above does not in general vanish because the charge flow unto the flux tube from polarization current associated with the field line motion can only be balanced, in this model, by a change of end-loss current. To change the end-loss current, the potential, $\tilde{\phi}_L$, across the sheath on a moving field line needs to change.

In the high collisionality regime the rate of charge build up by the perturbed end loss is determined by end current as given by Eq. (1). Taking into account that field lines are moving gives the relation,

$$\frac{\partial Q_d}{\partial t} \equiv -2J_\parallel = -2J_\parallel \left(\Phi_d(\mathbf{r}_\perp - \boldsymbol{\xi}) + \tilde{\phi}_d(\mathbf{r}_\perp - \boldsymbol{\xi}), T_d(\mathbf{r}_\perp - \boldsymbol{\xi}), n_d(\mathbf{r}_\perp - \boldsymbol{\xi})\right) \qquad (2)$$

where the factor of 2 comes from the contribution from two ends. Recall that we are assuming $J_\parallel(\Phi_d, T_d, n_d) = 0$ for the equilibrium. Using that $-i\Omega\boldsymbol{\xi}_d = -ic\mathbf{k} \times \mathbf{b}\,\tilde{\phi}_d/B$, the

end current is then

$$J_\parallel = \left[\tilde{\phi}_d(\mathbf{r}_\perp) + \boldsymbol{\xi}_d \cdot \nabla\Phi_d(\mathbf{r}_\perp)\right] \frac{\partial J_\parallel}{\partial \Phi} = \frac{\partial J_\parallel}{\partial \Phi} \frac{\omega B \xi_d}{c k_y} \ . \tag{3}$$

[The structure of the end current, given by Eq. (3) is quite general. For example in Ref. 10 it was noted that even when the collision frequency is not large, the perturbed end-current is given by $J_\parallel = [\tilde{\phi}_d(r) + \boldsymbol{\xi}_d \cdot \nabla\Phi_d(r)]\chi(\omega) = \omega B \xi_d \chi(\omega)/k_y c$ with $\chi(\omega)$ the appropriate frequency response that is determined from kinetic theory. In particular such a response is justified if $k_\parallel \lambda^e_{\rm mfp} \ll 1$ ($\lambda^e_{\rm mfp} \equiv$ electron mean free path) and if $k_\perp \rho \ll 1$ ($\rho \equiv$ ion Larmor radius) as well as in other circumstances.

If we assume that the field line motion is nearly flute-like, the charge accumulation due to the transverse ion polarization is in the limit $k_y \sim k_x \gg \nabla T_e/T_e$

$$\frac{\partial Q_p}{\partial t} = -\int \nabla \cdot \mathbf{j}_p \, ds \equiv -\nabla \cdot \int \frac{c n_e e}{\omega_{ci}} \frac{d}{dt} \frac{\mathbf{E}_\perp}{B} ds \approx -\frac{c k_\perp^2 e}{\omega_{ci} B} \int_{-s_d}^{s_d} ds \, n_e \frac{d\tilde{\phi}}{dt} \tag{4}$$

where $\omega_{ci} = e_i B/m_i c$, s is the distance along a field line.

The sum of Eq. (2) and Eq. (4) needs to vanish. Then using Eq. (3), we obtain,

$$\frac{k_\perp^2 e c}{\omega_{ci} B} \int_{-s_d}^{s_d} \Omega^2 \, n_e ds = -2i \frac{\partial J_\parallel}{\partial \Phi} \omega \approx -\frac{2ie^2 n_{ed} c_s \omega}{T_{ed}} \ .$$

If Ω is sufficiently small, and ω_E constant, we can set $\omega = \omega_E$ on the right-hand side, use the relationship, $e\partial\Phi_d/\partial x \approx \Lambda \, \partial T_d/\partial x$, and find

$$\Omega = \pm e^{i\pi/4} \left(\frac{-\omega_E}{\rho_{sd}^2 k_\perp^2 \tau_d}\right)^{1/2} \approx \pm e^{i\pi/4} \left(\frac{-\Lambda k_y \frac{\partial T_{ed}}{\partial x} \omega_{ci}}{\tau_d \, k_\perp^2 T_{ed}}\right)^{1/2} \tag{5}$$

with $1/\tau_d = 2n_{ed}c_s/\int n_e ds$ and $\rho_{sd}^2 = T_{ed} \, m_i c^2/e^2 \, B^2$. An unstable mode exists independent of the sign of $k_y \, \partial T_{ed}/\partial x$. In the subsequent sections we will study the properties of the mode more carefully.

III. Eigenmode Equation

In the low-beta limit, only the parallel component of the vector potential need be retained, so that

$$\tilde{\mathbf{B}} = \nabla \times \tilde{A}_\parallel \mathbf{b} = i\mathbf{k} \times \mathbf{b} \tilde{A}_\parallel \ . \tag{6}$$

where "~" indicates a perturbed quantity. The eigenmode equation is obtained from $\nabla\cdot\tilde{\mathbf{j}} = 0$, where we evaluate $\mathbf{j}_\perp$ and $j_\parallel$ from the Braginskii [9] two-fluid equations (electromagnetic) and an expansion in terms of $k_\parallel/k_\perp \sim k_\perp\rho \sim (\omega/\omega_{ci})^{1/2} \sim \epsilon$. The ϵ expansion is used to obtain explicit (drift) expressions for the fluid velocities perpendicular to $\mathbf{B}$. Hence, as in Hinton and Horton [11] , the current equation becomes

$$\nabla\cdot\mathbf{j} \cong \nabla_\perp\cdot\left[\frac{ne}{\omega_{ci}}\left(\frac{\partial}{\partial t}+(\mathbf{v}_E+\mathbf{v}_{pi})\cdot\nabla\right)\frac{c\mathbf{E}}{B}\right]+\nabla\cdot j_\parallel\mathbf{b}=0 \tag{7}$$

where $\mathbf{v}_{pj} = (c/n_jq_jB)\mathbf{b}\times\nabla p_j$, $\mathbf{v}_E = (c/B)\mathbf{E}\times\mathbf{b}$, and p_j is the pressure of species j, and where the perpendicular and parallel derivatives are defined relative to the direction of the equilibrium magnetic field. In Eq. (7) we have neglected the gyroviscous term as it does not contribute significantly in the subsequent equations. We also neglect here the curvature drift, as it has a small effect on the mode under consideration. From the components of the electron and ion momentum equations parallel to the equilibrium magnetic field and the lowest-order continuity equations (again assuming $\nabla_\parallel \ll \nabla_\perp$), we obtain

$$\begin{aligned}\frac{\partial j_\parallel}{\partial t}+\mathbf{v}_E\cdot\nabla j_\parallel + e\nabla_\parallel\left(n(u_i^2-u_e^2)\right)-\frac{ne^2}{m_e}(E_\parallel+\mathbf{v}_e\times\mathbf{B}\cdot\mathbf{b}_0/c)\\ =\frac{e}{m_e}\left[\nabla_\parallel p_e+n\alpha_T(\mathbf{B}\cdot\nabla T_e)/B\right]-\nu j_\parallel\end{aligned} \tag{8}$$

where $\mathbf{v}_e = \mathbf{v}_E + \mathbf{v}_{pe}$, u_j is the parallel flow velocity of species j, and we have used a cancellation between $\mathbf{v}\cdot\nabla$ terms and components of the stress tensor similar to those noted in Ref. 11. Linearizing Eq. (8), using Eq. (6) and its curl, and writing $\tilde{\mathbf{E}} = -i\mathbf{k}_\perp\tilde{\phi} - \mathbf{b}(\nabla_\parallel\tilde{\phi} - i\omega\tilde{A}_\parallel/c)$, we obtain the perturbed parallel current,

$$\begin{aligned}\tilde{j}_\parallel \cong \frac{k_\perp^2c^2}{4\pi}&\left[-i(\Omega-\omega_e^*-\alpha_T\omega_{eT}^*)+(k_\perp^2c^2/\omega_{pe}^2)(-i\Omega+\nu_e)\right]^{-1}\times\\ &\Big\{-\partial_s(\tilde{\phi}-\alpha_T\tilde{T}_e/e)+(en_0)^{-1}(\partial_s\tilde{p}_e+\alpha_T\tilde{n}\partial_sT_{e0})\\ &\quad+E_{\parallel0}(\tilde{n}/n_0)-4\pi[j_{\parallel0}\tilde{\nu}+\tilde{\mathbf{v}}_{\perp E}\cdot\nabla j_{\parallel0}]/\omega_{pe}^2\Big\}\end{aligned} \tag{9}$$

where $\tilde{T}_e$ is the perturbed electron temperature, $\alpha_T = 0.71$ is the thermal-force coefficient, n_0 is the equilibrium electron density, s is the distance along a field line, $\Omega = \omega - \omega_E$,

$\omega_E = c\mathbf{k} \times \mathbf{b} \cdot \nabla\Phi_0/B$, Φ_0 the equilibrium potential, $\omega_e^* = -\mathbf{k} \times \mathbf{b} \cdot \nabla(nT_e)/n\omega_{ce}m_e$, $\omega_{eT}^* = -\mathbf{k} \times \mathbf{b} \cdot \nabla(T_e)/\omega_{ce}m_e$, and $j_{\|0}$ is the equilibrium current. In writing Eq. (9), we have anticipated the result $\omega_{bi}/\Omega \ll 1$, where ω_{bi} is the ion transit frequency, and hence have dropped the u^2 terms.

Near the conducting end walls this parallel current impinges on the conductor and the form of the current is determined from the properties of the plasma sheath adjacent to the contacting wall, to be enumerated shortly. The sheath condition will provide a boundary condition to the eigenmode equation to be derived below, allowing the determination of the dispersion relation.

Note that, in writing Eq. (9), we are making a local approximation (Fourier analyzing in both x and y). This is not unreasonable since, unlike in the core of a tokamak, there are no special values of x (no analog of rational surfaces). On the other hand it fails for $k_x L_{Te} \sim 1$, and cannot describe effects of penetration into the closed-field-line region. A radial differential equation can be recovered from our treatment by unfolding $k_x \rightarrow i\partial/\partial x$; this is deferred to a future paper.

We adapt a "square-well" model in which the equilibrium quantities $(n_0, T_0, \Phi, \mathbf{B})$ are taken to be constant over the bulk of a field line but the end losses are determined by local values of the equilibrium quantities which are allowed to be different than the bulk values. From a simple equilibrium parallel electron heat equation we might expect the electron temperature to be nearly constant along a field line provided that the electron mean free path λ_{mfpe} satisfies $\lambda_{\mathrm{mfpe}}/L \gg \Lambda(m_e/m_i)^{1/2}$. In fact, the temperature measured in the SOL in a tokamak varies by a factor of several over its length (see for example a series of papers from the DIII-D group [8]), a fact which may be attributed to the violation of the above criterion near the divertor/sheath region as well as the combined effects of radiation, ionization, cross-field transport, and electron-ion energy exchange. However, for classical diffusion between regions of sources and sinks, $T^{7/2}$ varies linearly with distance along a field line, implying a temperature which is nearly constant over the bulk of the field line and falling sharply near the ends. This tendency is further accentuated by the localization of radiation and ionization losses near the ends. Hence the "square-well" approximation is reasonable. We shall also, for simplicity, neglect the term in Eq. (9) coming from the

gradient of the $j_{\|0}$ and the $\nabla_\perp \cdot j_\| \tilde{\mathbf{B}}/B$ term arising from the linearization of the $\nabla \cdot j\mathbf{b}$ term in Eq. (7). (The equilibrium current is in general non-zero. However, it is typically some modest fraction of env_{ti}. If the radial scale of $j_{\|0}$ is of the order of the SOL radial electron temperature scale length L_{Te}, we can verify *a posteriori* that the $j_{\|0}$ terms would tend to be small for typical parameters.) Finally, we shall neglect the radial gradient of the equilibrium rotation rate.

With these approximations the $\nabla \cdot \mathbf{j} = 0$ condition becomes:

$$\frac{\partial}{\partial s}\frac{\Psi k_\perp^2 c^2}{\Omega(\Omega - \omega_e^* - \alpha_T \omega_{eT}^*)}\frac{\partial[\tilde{\phi} - (\alpha_T \tilde{T}_e + \tilde{p}_e/n_0)/e]}{\partial s} + \frac{\omega_{pi}^2}{\omega_{ci}^2}k_\perp^2\left(1 - \frac{\omega_i^*}{\Omega}\right)\tilde{\phi} = 0$$

where $\Psi^{-1} = 1 + (k_\perp^2 c^2/\omega_{pe}^2)(\Omega + i\nu_e)/(\Omega - \omega_e^* - \alpha_T \omega_{eT}^*)$. We eliminate $\tilde{T}_e$ and $\tilde{p}_e$ using the electron continuity and temperature equations; if we temporarily neglect parallel thermal conductivity, then, to leading order, these equations are just $-i\Omega\tilde{T}_e + \tilde{\mathbf{v}}_{\perp E} \cdot \nabla T_e = 0$ and similarly for n. The $\mathbf{v}_{de}$ terms in the temperature equation cancel with a component of the thermal-gradient heat flux as noted in Ref. 11. Also, we have dropped the $\nabla_\| u$ terms from both the continuity and temperature equations, since, from the expression for $k_\|$ given below, it follows that such terms lead to corrections in the $\tilde{j}_\|$ response which are $\mathcal{O}(k_\perp \rho_s)$ with $\rho_s^2 = m_i c^2 T_e/e^2 B^2$. Now $k_\perp \rho_s$ must be small in order for our fluid equations to be valid if $T_i \sim T_e$; it can be verified *a posteriori* that $k_\perp \rho_s$ is in fact small at the most unstable wavelengths for physically interesting parameters. It follows that $\tilde{p}_e/p_0 = (\omega_e^*/\Omega)e\tilde{\phi}/T_e$ and $\tilde{T}_e/T_0 = (\omega_{eT}^*/\Omega)e\tilde{\phi}/T_e$. These relations can be easily obtained from guiding-center equations or more rigorously from fluid equations including diamagnetic flow, if FLR terms are included. Hence, the eigenmode equation in the bulk of the field line becomes

$$\frac{\partial}{\partial s}\frac{\Psi k_\perp^2 c^2}{\Omega^2}\frac{\partial \tilde{\phi}}{\partial s} + \frac{\omega_{pi}^2}{\omega_{ci}^2}k_\perp^2\left(1 - \frac{\omega_i^*}{\Omega}\right)\tilde{\phi} = 0 \quad . \tag{10}$$

In most of what follows, we shall usually consider the limit $\Psi = 1$.

In the $\Psi = 1$ limit ($k_\perp^2 c^2/\omega_{pe}^2 \ll 1$), $\tilde{T}_e/T_0 = (\omega_{eT}^*/\Omega)e\tilde{\phi}/T_e$ is the solution of the temperature equation even when the parallel and the gyrotropic heat conduction terms are retained. Hence Eq. (10) remains valid. In the opposite limit $k_\perp^2 c^2/\omega_{pe}^2 \gg 1$, the parallel heat conduction term is negligible compared to ΩT provided that $k_\perp^2 \rho_s^2(\Omega + \nu_e)/\nu_e \ll 1$,

which is typically true for the most important linear modes. Hence we take Eq. (10) as valid for both the electrostatic and electromagnetic regimes.

The symmetric solution to Eq. (10) is

$$\tilde{\Phi}(s) = \tilde{\Phi}_0 \cos k_{\|} s \tag{11}$$

with $k_{\|}^2 = \Omega(\Omega - \omega_i^*)/v_A^2 \Psi$.

Note that multiple species can be included as a sum over $\omega_{pj}^2/\omega_{cj}^2$ in Eq. (10) with j the various ion species. Hence Eq. (10) remains valid provided one interprets the ionic mass, atomic number, and diamagnetic drift frequency as the mean quantities defined at the end of Sec. I.

IV. End-Loss Physics

Equating the parallel current from the bulk with that crossing the sheath provides the boundary condition which closes Eq. (10) and allows determination of the dispersion relation. The form of the current crossing the sheath depends on the electron collisionality. For the case where electron collisions are sufficient to populate the velocity-space loss cone, the loss currents are similar to that given in Refs. 1 and 2, *i.e.*,

$$j_{\|} = enc_s \left[1 + \gamma_{si} - \frac{(1-\gamma_{se})v_{te}}{2c_s\sqrt{\pi}} \exp\left(-\frac{e\Phi}{T_e}\right) \right]_{s_d} \tag{12}$$

where c_s is the sound speed at the sheath, which for simplicity we take as $[(T_e + T_i)/m_i]^{1/2}$ and $v_{tj} \equiv (2T_j/m_j)^{1/2}$, and γ_{si} and γ_{se} are the coefficients for secondary-electron emission from ion and electron bombardment, respectively. (We shall restrict attention to $\gamma_{se} < 1$ to avoid discussion of double layer structures which would otherwise arise.) All quantities in this relation are to be evaluated on the plasma side of the sheaths, *i.e.* at $s = s_d \equiv \pm L/2$. Note again that these parameters are allowed to differ significantly from the bulk values; we shall give a prescription for self-consistently determining $T_e(s_d)/T_e(0)$ in Sec. V. In equilibrium we take $j_{\|} = 0$, and the equilibrium ambipolar potential $\Phi(s_d)$ then follows from Eq. (12). In fact we shall be interested below in the potential $\Phi(0)$ in the bulk of a field line; hence we must add to $\Phi(s_d)$ the potential drop across the pre-sheath. Hence we

obtain

$$\Lambda \equiv \left[\frac{e\Phi}{T_e}\right]_{s_d} = \frac{1}{2}\ln\left[\frac{m_i}{m_e}\left(\frac{1-\gamma_{se}}{1+\gamma_{si}}\right)^2 \frac{2T_e}{T_i+T_e}\frac{K_i^2}{4\pi}\right]_{s_d} \tag{13}$$

where $K_i \equiv \ln\left[\left(\Phi(0)-\Phi(s_d)\right)/T_{ed}\right]$. The constant K_i depends on the details of the pre-sheath model; in a simple model [13] with T_i small compared to T_e in the pre-sheath, $K_i = 2$, and is somewhat larger for finite T_i. Unless γ_{se} is close to unity, Λ is substantially larger than unity ($\Lambda \sim 4$). Note that a finite equilibrium current $j_\parallel \lesssim nec_s$ would not change this relationship appreciably.

Linearizing Eq. (12), we find that the perturbed current is given by

$$\tilde{j}_\parallel = \left[j_\phi\tilde{\phi} + j_{T_e}\tilde{T}_e + j_{T_i}\tilde{T}_i\right]_{s_d} \quad . \tag{14}$$

where $\hat{c}_s = c_s(1+\gamma_{si})$ and $j_\alpha \equiv \partial j_\parallel/\partial\alpha$.

The electrostatic potential at the end wall regulates the end-loss energy flux to the value

$$\begin{aligned} Q_{el} =& \frac{nv_{Te}}{2\pi^{1/2}}\exp\left(\frac{-e\Phi}{T_e}\right)\left[2T_e + e\Phi_0(1-\gamma_{se}) - \gamma_{se}T_{se}\right] \\ &+ n_i(c_s/K_i)\{T_i - \gamma_{si}T_{se} + \gamma_r[f_x(T_e+T_i) + f_i(\mathcal{E}_i - T_{ri} - T_{re})]\} \quad . \end{aligned} \tag{15}$$

where T_{se} is the temperature of recycled electrons, γ_r is the recycling coefficient, $\mathcal{E}_i$ is the ionization energy for recycled neutrals, T_{ri} and T_{re} are the mean temperatures of ions and electrons produced by ionization and charge exchange of recycled neutrals, and f_x and f_i are, respectively, the fraction of recycled neutrals ionized and charge-exchanged, respectively. Here we have assumed that the mean free path for recycled neutrals is longer than the sheath thickness but less than the perpendicular wavelength. In principle this equation provides a boundary condition for equilibrium and perturbed temperature equations. For most of the present work, however, we shall simply treat the equilibrium temperatures at the middle of the field line and at the sheath as prescribed constants. A discussion of a self-consistent determination is given in Sec. VI.

Linearizing the electron and ion portions of Eq. (15) and using the zero-equilibrium-current constraint, we find that, with the ordering $\omega_{bi} \ll \Omega$, the perturbed end-loss energy flux is negligible compared to the cross-field convective energy flux unless γ_{se} is very close

flux unless γ_{se} is very close to one. Hence, we find [at the sheath, and, in accord with the remarks following Eq. (10), everywhere along the bulk of the field line]

$$\begin{pmatrix} \tilde{T}_e \\ \tilde{T}_i \\ \tilde{n} \end{pmatrix} \cong -\boldsymbol{\xi} \cdot \begin{pmatrix} \nabla T_e \\ \nabla T_i \\ \nabla n \end{pmatrix} \quad . \tag{16}$$

where $\boldsymbol{\xi} = \tilde{\phi} c \mathbf{k} \times \mathbf{b}/B\Omega$.

We can substitute Eq. (16) into Eq. (14) to express the end wall current in terms of the fluctuating potential. Equating this result to Eq. (9) (with the $E_{\|0}$ and $\nabla j_{\|0}$ corrections dropped) gives the basic boundary condition for our analysis,

$$\begin{aligned} \Psi k_\perp^2 c^2 \frac{\partial(\tilde{\phi}/\Omega)}{\partial s}\Big|_{s_d} &= \frac{i\omega_{pe0}^2 L}{\tau v_{ted}^2}\left[\tilde{\phi} - \boldsymbol{\xi}\cdot\nabla T_e(j_{T_e}/j_\phi) - \boldsymbol{\xi}\cdot\nabla T_i(j_{T_i}/j_\phi)\right]_{s_d} \\ &\equiv \frac{i\omega_{pe0}^2 L\tilde{\phi}}{\tau v_{ted}^2\Omega}(\Omega + \omega_E) \end{aligned} \tag{17}$$

where $\tau^{-1} = 2n(s_d)\hat{c}_s/n_0 L$ with n_0 the density on the bulk of a field line of length $L = 2s_d$. Note that $\tau/(1+\gamma_{si})$ the ion confinement time. The quantity $\Omega + \omega_E$ is equal to the wave frequency ω and hence is independent of position. Also, in the MHD ($\Psi = 1$) limit, it is well known tha the dispalcement $\psi \propto \tilde{\phi}/\Omega_E$ cannot vary along a field line on a length scale short comared to v_A/Ω. Hence, for $k_\| \ell \ll 1$, where ℓ is the pre-sheath length, we can choose to evaluate $\tilde{\phi}/\Omega$ and $\Omega + \omega_E$ on the plasma side of the pre-sheath, so that Ω has the same meaning in Eq. (17) as in the eigenmode equation (10). (We assume that ω_E is constant outside of the sheath/pre-sheath region.) Then, since the $\mathbf{E}\times\mathbf{B}$ rotation is driven primarily by the gradient in T_{ed}, we write $\omega_E = -\omega_{eTd}^* \Lambda'$ where $\Lambda' \equiv d\Phi(0)/dT_{ed} = \Lambda + (T_{id}/2T_{ed})(1 - L_{Ted}/L_{Tid})/(1 + T_{id}/T_{ed})$ with $L_{Tid} = (\mathbf{b}\times\mathbf{k})\cdot\nabla \ln T_{id}/k_\perp$ and $L_{Ted} = (\mathbf{b}\times\mathbf{k})\cdot\nabla \ln T_{ed}/k_\perp$. Note that, while we have considered various atomic physics processes associated with secondary emission and charge exchange, the only effect which has a significant direct effect on the dispersion relation is secondary emission from ion bombardment (contained in the definition of τ, through $\hat{c}_s$). A similar analysis shows that radiation is unimportant for typical parameters. The other processes enter indirectly in that they affect the equilibrium parameters.

The inclusion of the ω^*_{eT} term, considered in Refs. 1 and 2, allows for a strong temperature gradient drive, particularly since Λ' is frequently a relatively large number and the temperature-gradient scale length L_{Te} which enters into ω^*_{eT} is typically very small in the SOL, $L_{Te} \sim 1$ cm.

If the collisionality is insufficient to justify Eq. (12), Eqs. (12), (13) and (15) should be replaced by their collisionless counterparts. To leading order, the dispersion relation is unchanged by this substitution, except indirectly through the resultant change in equilibrium parameters.

V. Dispersion Relation

Combining Eqs. (11) and (17) gives the dispersion relation

$$\frac{2\Omega(\Omega-\omega_i^*)\tan[k_\parallel(\Omega)L/2]}{k_\parallel(\Omega)L}+\frac{i\Omega Z}{\tau k_\perp^2\rho_s^2}\left[1-\frac{\omega^*_{eTd}}{\Omega}\Lambda'\right]=0 \tag{18}$$

where $\rho_s=[m_iT_e(s_d)]^{1/2}c/eB$, $k_\parallel(\Omega)$ is given following Eq. (11), and $\omega^*_{eTd}=\omega^*_{eT}(s=s_d)$.

We shall consider two extreme limits analytically and perform numerical calculations for intermediate regimes. The limits are: (1) a flute mode where $k_\parallel(\Omega)L \ll 1$; (2) a long system where $\mathrm{Im}\, k_\parallel(\Omega)L/2 \gtrsim 1$; additional modes with $k_\parallel(\Omega)L/2 \simeq \pi(\ell+1/2)$, where ℓ is an integer, are also derived. We shall see that, for the typical case $k_\perp^2c^2/\omega_{pe}^2 \ll 1$, the flute limit is satisfied at low beta and not-too-long connection lengths L. If we move to lower beta by decreasing the density, at some point the $k_\perp^2c^2/\omega_{pe}^2$ criterion becomes reversed and $k_\parallel$ ceases to increase with decreasing beta. Nevertheless, at that point, for typical tokamak parameters, the flute-mode criterion would be well satisfied.

If we first assume a flute mode then Eq. (18) simplifies to

$$\Omega(\Omega-\omega_i^*)+\frac{i\Omega Z}{k_\perp^2\rho_s^2\tau}\left[1-\frac{\omega^*_{eTd}}{\Omega}\Lambda'\right]=0 \tag{19}$$

Instability is readily inferred from Eq. (19). To write the results compactly we normalize Eq. (19) to the form,

$$\hat{\Omega}^2+\hat{\Omega}[i/\hat{k}^2+\hat{k}\delta]-i/\hat{k}=0 \tag{20}$$

where $\delta=[T_{i0}/T_e(s_d)](L_{Te}/L_{pi}\Lambda')/Z$, with L_{pi} the radial ion pressure-gradient scale length (*i.e.* that which enters the definition of ω_i^*), and the dimensionless frequency and

wavenumber are given by $\hat{\Omega} = (\Omega/\Omega_{*0}\Lambda')\nu^{-1/3}$ and $\hat{k} = (k_\perp \rho_s)\nu^{-1/3}$, with $\nu = Z/\tau\Lambda'\Omega_{*0}$, $\Omega_{*0} = (k_y/k_\perp)\omega^*_{eTd}|_{k_y\rho_s=1} \equiv (k_y/k_\perp)c_{se}/L_{Te}$, and $c_{se} = [T_e(s_d)/m_i]^{1/2}$. Solutions for $\mathrm{Im}\,\hat{\Omega}$ as a function of $\hat{k}$ for various values of δ are shown in Fig. 1. For $\delta = 0$, the maximum value of $\hat{\gamma} \equiv \mathrm{Im}\,\hat{\Omega}$ is $\hat{\gamma} = \hat{\gamma}_m = 0.38$, which is achieved when $\hat{k} = \hat{k}_m \cong 1.8$. At this value of $\hat{k}$, $\mathrm{Re}\,\hat{\Omega} = \mathrm{Re}\,\hat{\Omega}_m \cong 0.52$. We also note that $\max(\hat{\gamma}/\hat{k}^2) = 0.343$. For δ large, the $\hat{\Omega}^2$ term can be neglected for the unstable mode, and we find $\hat{\gamma}_m = (2^{2/3}/3)\delta^{-1/3}$ at $\hat{k}_m = 2^{1/6}\delta^{-1/3}$. Note that $k_y/k_\perp$ does not appear in Eq. (20); hence the maximum dimensionless growth rate is independent of $k_y/k_\perp$. Upon translation back to physical variables, we see that, for other parameters fixed, the growth rate scales as $(k_y/k_\perp)^{2/3}$; thus the actual growth rate is maximized in the limit $k_x \to 0$. Hence, in all of the expressions which follow, Ω_{*0}, ν, etc., are to be evaluated with $k_y/k_\perp \to 1$.

At the maximum growth rates $\mathrm{Im}\,\hat{\Omega} \sim \mathrm{Re}\,\hat{\Omega}$. Hence we can expect strong turbulence with mixing-length theory being appropriate so that thermal diffusivity is $\chi \approx \hat{\gamma}_m/\hat{k}_m^2$, where $\hat{k}_m$ is the wavelength at $\hat{\gamma} = \hat{\gamma}_m$. [Note, however, that $\max(\hat{\gamma}/\hat{k}^2)$ and $\hat{\gamma}_m/\hat{k}_m^2$, which are two commonly-used mixing-length diffusivity estimates, differ by nearly a factor of three; this is an indication of the uncertainty involved in the use of a mixing-length estimate.] In the limit of both small and large δ, the scaling of the solution is completely determined (no scaling at all in the dimensionless variables for small δ, and the 1/3-power scalings for large δ). Thus we can explicitly write the mixing-length diffusivity in physical variables as

$$\frac{\gamma}{k^2} \approx \frac{c_{se}\rho_s^2}{L_{Te}}\Lambda' \left(\frac{\Lambda' L c_{se} n_0}{2L_{Te}c_s n(s_d)(1+\gamma_{si})Z}\right)^{1/3} \frac{\hat{\gamma}_m}{\hat{k}_m^2} \tag{21}$$

if $\delta = [T_{i0}/T_e(s_d)](L_{Te}/L_{pi}\Lambda')/Z \ll 1$, while

$$\frac{\gamma}{k^2} \approx \frac{1}{3}\frac{c_{se}\rho_s^2}{L_{Te}}\Lambda' \left(\frac{T_{i0} L c_{se} n_0}{2T_{ed}L_{pi}c_s n(s_d)(1+\gamma_{si})Z}\right)^{1/3} \tag{22}$$

if $\delta \gg 1$. Here, $c_{se} = [T_e(s_d)/m_i]^{1/2}$.

In Fig. 2 we plot $\hat{\gamma}_m$, $\mathrm{Re}\,\hat{\Omega}_m$, k_m and $\hat{\chi} = \hat{\gamma}_m/\hat{k}_m^2$ vs. δ. The predicted weak variations with δ are evident at large δ. Note that, for the experimentally interesting case $\delta \sim 1$, $\hat{\gamma}_m$ is barely changed from the $\delta = 0$ limit, while k_m and $\mathrm{Re}\,\hat{\Omega}_m$ decrease; hence $\hat{\chi}$ increases appreciably. For negative $\delta \sim -1$ (which can occur when either the electron temperature

profile or ion-pressure-gradient profile is inverted), $\hat{\gamma}_m$ decreases somewhat while Re $\hat{\Omega}_m$ and k_m increase, the mode becomes more nearly real and $\hat{\chi}$ moderately decreases.

For later reference, we restore numerical constants and display the diffusivity in practical units,

$$\chi_{ml} \approx \frac{2.3\mathrm{m}^2/\mathrm{sec}}{L_{Te}(\mathrm{cm})^{4/3}}(T_e(s_d)/25\,\mathrm{eV})^{3/2}(\Lambda'/4)^{4/3}(L_\parallel/40\,\mathrm{m})^{1/3}$$
$$[1.5/(1+\gamma_{si})Z]^{1/3}A^{1/2}(2\,\mathrm{T}/B)^2(n_0/n_d)^{1/3}[2T_e/(T_e+T_i)]_d^{1/6}G \qquad (23)$$

where $G \sim 1$ is the ratio of the actual $\hat{\chi}$ to that for $\delta = k_\parallel = 0$. For $\delta \approx K_T \approx 1$ (parameters typical of DIII-D; here K_T is the finite-$k_\parallel$ parameter defined two paragraphs below), $G \approx 2$. Interestingly, for $K_T \approx 2$ and $\delta \approx 1$, the finite-$k_\parallel$ and finite ω_i^* effects nearly cancel to give $G \approx 1$. On the other hand, for large K_T (typical for reactor-grade parameters), the effects can be additive, as will evident from the discussion below.

It also follows from mixing-length theory that the level of potential fluctuation should be $e\tilde{\phi}/T \approx 1/k_y L_{Te}$.

In Ref. 14, it is shown that, for the nonlinear equations appropriate in the flute limit, it is possible to completely remove all parameters in the large and small δ limits, just as in the linear case, and that, as a consequence, mixing-length scaling is in fact rigorously correct in these limits. A caveat in this analysis is the neglect of the energy end-loss terms (as has been done here, also), which is justified for frequencies near the maximum growth rate, but could be problematic if nonlinear effects result in significant wave energy at frequencies near or below the ion transit frequency.

Next, we consider finite $k_\parallel$ effects. Introducing the same dimensionless variables used in the flute equation, we can rewrite the dispersion relation, Eq. (18), in the form

$$(\hat{\Omega}^2 + \delta\hat{k}\hat{\Omega})\mathcal{T} + \frac{i\hat{\Omega}}{\hat{k}^2} - \frac{i}{\hat{k}} = 0 \qquad (24)$$

where $\mathcal{T} \equiv (2/k_\parallel L)\tan(k_\parallel L/2)$ and $k_\parallel L/2$ satisfies

$$k_\parallel L/2 = K_T\left(\hat{\Omega}^2 + \delta\hat{k}\hat{\Omega}\right)^{1/2} \quad . \qquad (25)$$

Here, $K_T = (1+\gamma_{si})Z(\beta_d n_d/2n_0)^{1/2}\nu^{-2/3}$ measures the importance of finite $k_\parallel$ effects and is also the only direct way that the plasma beta [$\beta_d \equiv 8\pi n_d(T_{ed}+T_{id})/B^2$] enters

the calculation. Note that finite $k_\parallel$ introduces only one new parameter, namely K_T. For typical present-day tokamak scrape-off layers, such as that of DIII-D, or ITER, K_T is in the range 1 – 1.5. For a reactor-grade machine, K_T can be large; for example, for the nominal ITER parameter set discussed in Sec. VII, $K_T \approx 5$. This distinction is quite important, as will be seen shortly.

For small K_T, we can expand the tangent and replace $\mathcal{T}$ by 1 to obtain the flute limit analyzed above. There are additional roots with $k_\parallel L/2 \approx n\pi$. At the maximum growth rate, these roots have high real frequency and wavenumber, $\max \hat{\Omega} \propto n\pi/K_T$, $k_m \propto n\pi/K_T$, and vanishing growth rate, $\hat{\gamma}_m \propto (K_t/n\pi)^2$. (For $\delta = 0$, the proportionality constants are 1, 2, and 1/4, respectively.) These roots are nonetheless somewhat interesting because of their connection to high-K_T roots with $k_\parallel L/2 \approx (2n+1)\pi/2$ as discussed below.

We can perform asymptotic analyses to determine analytically maximum growth rates for large K_T. There are several distinct types of roots in this limit. We restrict attention to the normally occurring case $\delta > -1$. We present here the results of the analysis; derivations are given in the Appendix. First, and most significantly, there are roots for which the maximum growth rate occurs when $\theta(\hat{\Omega}) \equiv k_\parallel L/2 \approx \ell\pi/2$, with ℓ an odd integer. For these roots, the maximum growth rate occurs at $\hat{k} = \hat{k}_{\ell m} = \ell(\pi/2)K_T^{-1}[1/(1+\delta)]^{1/2}$, at which point $\hat{\Omega} = \hat{k} + \tilde{\Omega}_{\ell m}$, with

$$\tilde{\Omega}_{\ell m} \approx (-1+i)(\ell\pi/2)^{3/2} K_T^{-5/2} \frac{1}{[2+\delta]^{1/2}(1+\delta)^{1/4}} \quad . \tag{26}$$

The growth rate is an increasing function of ℓ, but the formula is only valid for $\ell \lesssim K_T$. There is a higher-$k_\parallel$ mode with $\mathrm{Im}\,\theta \gg 1$, and which is thus localized near the ends of the field line. For the particular case $\delta = 0$, the maximum growth rate is $\mathrm{Im}\,\hat{\Omega}_m \approx (3/4)K_T^{-1} \ln K_T$, and occurs for $\hat{k} \approx K_T^{1/2}$, $\hat{\Omega}_r \cong K_T^{1/2}/2$. Note that this maximum growth rate is less than that obtained from Eq. (26) for $\ell \sim K_T$. Finally, there are modes for which $\mathrm{Re}\,\theta \sim \mathrm{Im}\,\theta \sim 1$ and the second term in Eq. (24) is negligible. We shall refer to these as large-wavenumber modes, since $\hat{k}_m$ is larger than for the other roots. There is a series of roots corresponding to different branches of $\tan^{-1}$. For $\delta = 0$, the first three such modes are, after maximizing the growth rates, $\hat{\Omega}_m \cong (1.042 + 0.6013i)K_T^{-1}$ at $\hat{k}_m = 0.6616K_T^2$, $\hat{\Omega}_m \cong (3.9893 + 1.0287i)K_T^{-1}$ at $\hat{k}_m = 0.2353K_T^2$, and $\hat{\Omega}_m \cong (7.1032 + 1.227i)K_T^{-1}$ at

$\hat{k}_m = 0.1371 K_T^2$. The growth rate is a weakly increasing function of mode number, a trend which continues for at least two more modes beyond the ones reported above. For $\delta \neq 0$, the first such mode maximizes when $\theta \to \pi/2$, but is nonetheless distinct from the first of the $\ell\pi/2$ roots listed above; in particular, it has a smaller growth rate, $\hat{\gamma}_m \cong \pi^2/2\delta K_T^3$, and, from numerical comparisons, a higher wavenumber $\hat{k}_m$. The second and third roots are immediately distinct from the $\ell\pi/2$ roots after maximizing, and are at $\hat{\Omega}_m \cong (145.6 + 47.61i)/\delta^{-1} K_T^{-3}$ at $\hat{k}_m = 0.1385 K_T^2$, and $\hat{\Omega}_m \cong (526.4 + 198.1i)/\delta^{-1} K_T^{-3}$ at $\hat{k}_m = 0.1066 K_T^2$, respectively. Note that, for $\delta = 0$, these are the fastest-growing modes, whereas, for $\delta \neq 0$, they grow much more slowly than the $\ell\pi/2$ modes. In either case, the transport, as measured by the mixing-length diffusivity $\hat{\chi} = \hat{\gamma}_m/\hat{k}_m^2$, is more important for the $\ell\pi/2$ modes, as $\hat{\chi} \sim (\ell K_T)^{-1/2}$ for the $\ell\pi/2$ modes and $\hat{\chi} \sim K_T^{-5}$ and $K_T^{-7}\delta^{-1}$ for $\delta = 0$ and $\delta \neq 0$, respectively. The last ($\delta \neq 0$) scaling applies only for $\ell > 1$, but the conclusion is applicable to $\ell = 1$ as well, because of the aforementioned numerical evidence concerning $\hat{k}_m$ and the analytic $\hat{\gamma}_m$ expressions. The conclusion is that for large K_T, the $\ell\pi/2$ modes for $\ell \lesssim K_T$ dominate the transport, and the (dimensionless) mixing-length thermal diffusivity $\hat{\chi}$ should then be of the order $\hat{\chi} \sim \sum_\ell (\mathrm{Im}\,\tilde{\Omega}_{\ell m}/\hat{k}_{\ell m}^2) \approx 1$, where the sum runs up to $\ell \sim K_T$.

We explore intermediate-K_T values and the connection between the small- and large-K_T solutions by solving Eqs. (24)–(25) numerically. For $\delta = 0$, the flute mode ($\theta \to 0$ as $K_T \to 0$) connects on to the $\theta_m = K_T \omega_m \cong 1.042 + 0.6013i$ mode at large K_T; the $\pi/2$ mode emerges from it as a distinct maximum, finitely removed in $\hat{k}$, at K_T around 3.3. For higher K_T, a scan of $\hat{\Omega}$ vs. $\hat{k}$ reveals two distinct peaks and a smooth connection between, suggesting that the two maxima are separate maxima of the same root of the dispersion relation rather than two distinct roots. The real and imaginary parts of $\hat{\Omega}_m$, $\hat{k}_m$, and the mixing-length diffusivity $\chi_m = \hat{\gamma}_m/\hat{k}_m^2$ are plotted as functions of K_T for these two branches in Fig. 3. The higher-harmonic solutions in the $K_T \to 0$ limit appear as distinct roots; that is, at a given $\hat{k}$, one can switch between them by supplying different initial guesses to the numerical root finder. The $\theta = \pi$ root for $K_T \to 0$ matches smoothly on to the $\theta \approx 4 + i$ root at large K_T, with the $3\pi/2$ root pealing off at $K_T \approx 5.3$. This is shown in Fig. 3. For $\delta = 1$, the $\theta \approx 0$ small-K_T root connects smoothly to the $\pi/2$

large-wavenumber root at large K_T, and the $\theta = \pi$ root at small K_T connects on to the $\theta \cong 4.55 + .73i$ root (second of the large-wavenumber roots) at large K_T, as shown in Fig. 4. As was the case for $\delta = 0$, the $\ell\pi/2$ roots emerge from the large-wavenumber root with a distinct maxima in the growth rate at moderate K_T. A curiosity is that, for the one value of negative δ explored (-0.25), the flute mode appears to directly connect on to the (small-wavenumber) $\pi/2$ mode rather than the high-wavenumber root.

A significant feature of the $\ell\pi/2$ roots is that, unlike the flute limit at small K_T or the harmonic large-wavenumber ($\mathrm{Re}\,\theta \sim \mathrm{Im}\,\theta \sim 1$) roots at large K_T, $\hat{\gamma}_m \equiv \mathrm{Im}\,\hat{\Omega}_m$ is small compared to $\mathrm{Re}\,\hat{\Omega}_m$.

For typical present-day experimental situations where $K_T \approx 1$, $\hat{\Omega}_m$, $\hat{k}_m$ and $\hat{\chi}$ are only moderately changed from their $K_T \to 0$ limits; in particular, $\hat{\chi}$ is moderately reduced. Also, for $K_T \lesssim 2$, a single mode (the one which connects smoothly to the flute mode in the $K_T \to 0$ limit) is important, as measured by either growth rates or mixing-length diffusivity estimates. On the other hand, for large K_T, a number of distinct modes can appreciably contribute, possibly rendering the mixing-length diffusivity estimate larger than in the flute limit. This will be seen explicitly in the ITER example described in Sec. VII. This is the significant distinction between large and small values of K_T to which we alluded earlier.

We conclude this section with a qualitative discussion of the spectrum and the relationship between the fluctuating quantities. If we retain the dominant nonlinear effect (nonlinear $\mathbf{E} \times \mathbf{B}$ convection) and energy end-loss (linearized, and to leading order in powers of $1/\Lambda'$) and neglecting ∇p_i, we find that, in the flute limit, the current-conservation and energy equations are identical with the dissipationless Hasegawa-Wakatani equations [15] after rescaling of variables. (Neglecting the energy-endloss terms corresponds to the small-$\overline{C}_1$, or hydrodynamic, limit of the equations as given in Ref. [15].) Hence we can expect an inverse cascade of energy to long wavelengths, implying broad frequency and wavenumber spectra extending from the most unstable frequency downward from the most unstable frequency and wavenumber. Since in the nonlinear state the linear terms should still be in approximate balance, we expect the relationship between fluctuating fields to be roughly as in linear theory, *i.e.*, $\tilde{n}/n$, $\tilde{T}_e/T_e$, $\tilde{T}_i/T_i$ and $e\tilde{\phi}/T_e$ should be approximately

in the ratio $1/L_n$ to $1/L_{Te}$ to $1/L_{Ti}$ to $\Omega/\omega^*_{eTd}L_{Te}$, respectively, and they should all be approximately in phase. (Note that, for frequencies well below that at which maximum growth occurs, the frequency is nearly real and hence the aforementioned statement about phases has some meaning.) Since (see next section) we expect L_{Ti} and L_n small compared to L_{Te} and since Ω/ω^*_{eTd} $(= \Lambda\hat{\Omega}/\hat{k})$ is somewhat larger than unity at frequencies below that of the maximum growth rate (by a factor approaching Λ' at frequencies well below), we expect $e\tilde{\phi}/T_e$ to be largest, then $\tilde{T}_e/T_e$, and finally $\tilde{n}/n$ and $\tilde{T}_i/T_i$ in a relative order that depends on details.

VI. Self-Consistent Transport

The scale lengths L_{Te}, L_{Ti} and L_n can be determined self-consistently by equating the time $\tau_\perp$ for heat or particles to diffuse transverse to the magnetic field a distance L_{Te} (or L_{Ti} or L_n) to the axial lifetime. For the L_{Te} calculation, for example, $\tau_\perp = L^2_{Te}/\chi$ and the axial lifetime $\tau_\parallel$ is defined by the relationship $\tau_\parallel = (3/2)\langle nT\rangle L/Q_{el}$ with Q_{el} the end-loss heat flux and $\langle\ \rangle$ denoting a field-line average. (This procedure yields a scale length identical with that obtained from solving an equilibrium energy equation $\partial_x\chi\partial_x T = \nu_E T$ with a constant thermal diffusivity and a constant loss rate ν_E). In principle, the scale lengths which appear in the definition of $\tau_\perp$ are mid-field-line scale lengths, whereas in the diffusivity expressions L_{Te} refers to the scale length at the sheath. However, since we have dropped comparable geometrical factors elsewhere in making our "square well" approximation, there is little significance in retaining such a distinction. For electron temperature the axial lifetime is $\sim L/c_s\Lambda$ while for density (if we neglect recycling) and ion temperature the axial lifetime is $\sim L/c_s$. Assuming that the scaling for the transport coefficients for electron and ion temperature and density are given by the mixing-length formulas for χ in the flute-mode limit [Eqs. (21) and (22)], we then find, for either large or small δ,

$$
\begin{aligned}
L_{Te} &\sim L_{pi}\Lambda^{-1/2} \sim L^{2/5}\rho_s^{3/5}\lambda_t^{3/10}\lambda_n^{2/5}(\Lambda/Z)^{1/10}[T_e/(T_e+T_i)]^{1/5}\hat{\delta}^{1/10} \\
\gamma &\sim \left(c_{se}/\rho_s^{2/5}L^{3/5}\right)[(T_e+T_i)/T_e]^{3/10}\lambda_t^{-1/5}(\Lambda/\lambda_n)^{3/5}Z^{2/5}\hat{\delta}^{-2/5} \\
k_\perp\rho_s &\approx (\rho_s/L)^{1/5}[(T_e+T_i)/T_e]^{1/10}\lambda_t^{-1/5}\lambda_n^{-3/5}(Z/\Lambda)^{3/10}\hat{\delta}^{-3/10}
\end{aligned}
\tag{29}
$$

$$k_\perp L_{Te} \sim (\tilde{T}_e/T_e)^{-1} \sim \left(L\lambda_n\lambda_t^2 Z^2/\rho_s\Lambda\right)^{1/5} [T_e/(T_e+T_i)]^{1/10}\hat{\delta}^{-1/5}$$

$$\chi_e \sim \rho_s c_{se}(\rho_s/L)^{1/5}[(T_e+T_i)/T_e]^{1/10}\lambda_t^{-2/5}\Lambda^{6/5}(\lambda_n Z)^{-2/5}\hat{\delta}^{1/5}$$

Here, $\lambda_t = T_e(s=0)/T_e(s_d)$, $\lambda_n = n(s=0)/n(s_d)$, and unsubscripted temperatures are evaluated at the sheath. In these expressions, $\hat{\delta} \sim$ const. for $\delta \ll 1$ and $\hat{\delta} \sim \delta$ for $\delta \gg 1$, and $\delta \sim \Lambda^{-3/2}T_{i0}/T_{es}$.

These results show the self-consistency of our assumptions viz: $k\rho_i \ll 1, kL_{Te} > 1$. Further the diffusion is quite high, *e.g.* the thermal diffusivity in Eq. (29) is reduced only by a factor $(\rho_s/L)^{1/5}\Lambda^{6/5}$ from Bohm; in fact, when numerical factors are taken into account (including the usual factor of 1/16 in Bohm diffusion), the diffusivity can be comparable to or exceed Bohm. The scale lengths in the scrape-off layer can then be many ion Larmor radii thick even with a rapid axial loss.

If we include recycling, the particle axial lifetime is increased by a factor of $(1-\gamma_r)^{-1}$ over the estimate given above, and we would expect $L_n \sim (1-\gamma_r)^{-1/2}L_{Ti}$ if γ_r were constant. If we account for the temperature dependence of γ_r, then γ_r varies on the same scale as T_e, and hence we would expect to see a density variation on the same scale as the T_e variation.

Restoring numerical constants, retaining all T_e terms in Eq. (15) (but neglecting T_{se} and T_{re}, and also introducing radiative loss as a fixed multiple of F_r of the input power (and assumed distributed in radius in proportion to the energy end loss), we find in particular that

$$L_{Te}(cm) = L_1 \equiv \left[\frac{\chi_1}{2}\frac{\langle nT_e\rangle}{nT(s_d)}\frac{L}{\hat{c}_s(s_d)}\frac{1-F_r}{\Lambda+[2/(1-\gamma_{se})]+\gamma_r f_x/(1+\gamma_{si})}\right]^{3/10} \tag{30}$$

where $\chi_1 = \chi_{ml}(L_{Te} = 1\text{cm})$ in cm^2/sec.

These results are also demonstrated in the following quantitative calculations, done for a limited plasma ($L =$ const). We solve the following model equations in the scrape-off layer:

$$\frac{\partial}{\partial t}n = \frac{\partial}{\partial x}\chi\frac{\partial}{\partial x}n - \frac{2nv_f}{L} \quad , \tag{31}$$

$$\frac{3}{2}\frac{\partial}{\partial t}nT_j = \frac{3}{2}\frac{\partial}{\partial x}\chi\frac{\partial}{\partial x}nT_j - \frac{2nv_f}{L}\alpha_{\varepsilon j}T_j \quad , \qquad j = e,i \quad , \tag{32}$$

where $v_f = [(\alpha_i T_i + \alpha_e T_e)/m_i]^{1/2}$ is an effective flux velocity, and $\alpha_{\mathcal{E}j}$ and α_j are coefficients which depend on the flux model. The diffusion coefficient χ is taken to be $\chi = AT_e^{1/3}(\partial T_e/\partial x)^{4/3}$ with $A = \hat{\chi}\Lambda'^{4/3}(c_{se}L/2v_f)^{1/3}c_{se}\rho_s^2/T_e^{5/3}$ with $\hat{\chi} = \max(\hat{\gamma}/\hat{k}^2)$. The value of $\hat{\chi}$ depends on δ, and is 0.343 for $|\delta| \ll 1$, $0.529\delta^{1/3}$ for $\delta \gg 1$, and 0 for $\delta \leq -1$. We interpolate for $\delta \geq -1$ using the prescription:

$$\hat{\chi} \approx \frac{\delta + 1}{3(1 + \delta/2)^{2/3} - 0.087} \,. \tag{33}$$

We plot, in Fig. 5, the stationary solutions of Eqs. (31) and (32). We used the following parameter values: $T_{e0} = T_{i0} = 25$ eV (here, the subscript 0 denotes the value on the separatrix $x = 0$), $L = 20$ m, $B = 2$ T, $\Lambda' = 4$, atomic mass = 2 and $\alpha_{\mathcal{E}i} = 2, \alpha_{\mathcal{E}e} = \Lambda' + 2, \alpha_i = \alpha_e = 1$. We also plot in Fig. 5 the analytic stationary solution for T_e for the case $n = \text{const}$, $T_i = \text{const}$, $\alpha_e = 0$, (the coefficient A is then independent of x,) which is

$$T_e = T_{e0}(1 - x/x_0)^2 \quad , \qquad x \leq x_0 \quad , \tag{34}$$

where $x_0 = (9\hat{\chi}\rho_{s0}^2/\alpha_{\mathcal{E}e})^{3/10}(\Lambda' c_{se}(0)L/v_f)^{2/5}$.

These results show that, for the model, the density variation is in fact nearly as fast as the electron temperature variation, while the ion temperature falls off more slowly. Nevertheless, the analytic estimate for the electron temperature profile reproduces the numerical solution fairly well.

An additional limit for which $T_e(x)$ can be obtained analytically is the case $\alpha_i = 0$, which would apply if either $T_i \ll T_e$ or if the electron-ion collisionality [neglected in Eqs. (32)] were sufficiently high to force $T_e \approx T_i$. In the latter case one would add the electron and ion versions of Eq. (32) to eliminate the collisional equilibration term. The solution in this case is

$$T_e = T_{e0}(1 - x/x_1)^{10/3} \tag{35}$$

with $x_1 = (9\hat{\chi}\rho_{s0}^2/\alpha_{\mathcal{E}e})^{3/10}(\Lambda' L/2)^{2/5}$.

Next, we return to the more general situation of diverted or limited plasmas and look for a self-consistent scaling of parameters (temperatures, scale lengths, etc., but not detailed profile shapes) as a function of a specified input power. This is akin to the

calculations of Barr [16], but employing our physics-based thermal diffusivity expressions (vs. Barr's use of $\chi_e = \text{const}$).

Tokamak scrape-off layers typically have mean free paths comparable to the distance along a field line to the nearest divertor or limiter. Consequently analytic expressions based on either short- or long-mean-free-path approximations are marginal. However, as long as the collisionality is large enough to justify the collisional form of the energy end loss [Eq. (15)], then the collisionality enters only in the determination of λ_t, the ratio of the mid-field-line to sheath electron temperature. As Barr noted, use of the collisional parallel heat conductivity yields the correct λ_t (*i.e.*, 1) in the long-mean-free-path limit, and of course is also accurate in the short mean-free-path limit, but is erroneous (underestimates λ_t) in between. Following Barr, we account for this by employing collisional equations with a reduced thermal conductivity (1/2 the collisional value) for the case of interest where the mean free path is comparable to the system length.

The goal of this analysis is to solve for L_{Te}, T_{e0}, T_{es}, and λ_n in terms of the input power P and the mid-field-line density. The equations to be solved are conservation of energy continuity of perpendicular heat flux across the separatrix, the parallel heat conduction equation (modified as discussed above), and an equation relating the pressure at the sheath to the mid-field-line pressure. We also follow Barr in assuming rapid electron-ion equilibration at least near the pre-sheath and so take $T_{ed} = T_{id}$. The analysis which follows applies to single-null or double-null divertor configurations; for double-null, the analysis applies separately to the inner and outer scrape-off layers; P is then the power emerging into the SOL under consideration.

We assume that the power entering the SOL is that crossing the separatrix. Then energy conservation implies that, in steady state, the input power equals the sum of the energy end-loss flux integrated over the width of the scrape-off layer plus the power radiated, or of the field line (the collisional flux at the end of the field line must equal the heat flux crossing the sheath) implies

$$PB(1 - F_r)/4\pi RB_{p0}L_T = (nT\hat{c}_s)_d\eta \quad , \tag{36}$$

where η is the multiplier of T which gives the energy removed per escaping e-i pair [in

the absence of secondary emission and recycling, $\eta \approx \Lambda + 3$; more generally, see Eq. (15)], and F_r is the fraction of the input power radiated in the SOL. As before, the subscript d denotes a value at the sheath while the subscript 0 denotes a mid-field-line value.

Continuity of the radial heat flow across the separatrix implies that

$$P = 2\pi R \chi n_0 T_0 (\langle B_p \rangle / B_{p0}) L_{pol} / L_{Te} \quad , \tag{37}$$

where L_{pol} is poloidal length of a SOL field line. Note that eliminating P between Eqs. (36) and (37) and solving for L_{Te} yields an equation effectively equivalent to Eq. (30).

Finally, the connection between input power P, temperature, and parallel heat flow is made via the classical heat conduction equation, integrated along the magnetic field line. Following Barr, we assume that the heat source on a field line can be approximated as localized at the middle of the field line. Then the classical heat-conduction equation yields

$$\kappa_{\|} \left[T_0^{7/2} - T_{ed}^{7/2} \right] \approx (7/4)(1 - F_r/2) L_{\|} P B / 4\pi R B_{p0} L_{Te} \quad , \tag{38}$$

We supplement these equations by the assumption that the pressure at the sheath is a fixed fraction f_P of the mid-field-line pressure.

We solve Eqs. (36) and (37) for T_{e0} and L_{Te} in terms of λ_t, using the form for χ given by Eq. (23). We obtain the scalings

$$L_{Te}(\mathrm{cm}) \approx 0.5 (A\Lambda')^{1/3} \left[(1 - F_r) B / B_{p0} \eta \right]^{5/12} \left(\langle B_p \rangle G L_{pol} / B_{p0} \lambda_t \right)^{1/4} (L_{\|}/Z)^{1/12}$$
$$(P/n_{19}R)^{1/6} \left[B f_p (1 + \gamma_{si}) \right]^{-1/2} \tag{39}$$

$$T_{e0}(\mathrm{eV}) \approx 78 A^{1/9} \left[B/(1 + \gamma_{si}) f_p \right]^{1/3} \left[(1 - F_r) B / B_{p0} \eta \right]^{7/18} \lambda_t^{1/2}$$
$$(B_{p0} / \langle B_p \rangle L_{pol} G)^{1/6} (Z/L_{\|})^{1/18} \Lambda'^{-2/9} (P/n_{19}R)^{5/9} \tag{40}$$

where A is the atomic mass. Here all lengths are in meters except for L_{Te} and B is in Tesla. Since, in obtaining these results, we have approximated the two-dimensional SOL equilibrium by a essentially a point model, the numerical values should be interpreted as radially averaged values.

The equation for λ_t is then obtained by substituting Eq. (40) into Eq. (38),

$$f_\kappa \lambda_t^{7/4} (1 - \lambda_t^{-7/2}) \approx 1.05 \times 10^{-4} \log \lambda \frac{1 + Z_{\mathrm{eff}}}{2} Z^{-7/36} \left(G L_{pol} \frac{\langle B_p \rangle}{B_{p0}} \right)^{7/12} \left(\frac{\eta}{1 - f_r} \right)^{49/36}$$
$$\left(\frac{(1 + \gamma_{si}) f_p}{B} \right)^{7/6} (\Lambda')^{7/9} \left(\frac{L_{\|} n_{19} R}{P} \right)^{43/36} A^{-19/45} \left(\frac{B_{p0}}{B} \right)^{13/36} \tag{41}$$

where f_κ is the factor by which parallel heat conductivity is to be reduced to account for finite mean-free-path effects (1/2 for our applications), and $Z_{\rm eff}$ is the effective atomic number $\sum_j n_j Z_j^2 / \sum n_j Z_j$ (which is distinct from Z, which is to be interpreted as the average ionic atomic number as discussed at the end of Sec. III). We solve Eq. (41) by a numerical root search procedure. A simple scaling can be obtained by dropping the $\lambda_t^{-7/2}$ term, but this is usually not justified for typical SOL parameters (as the mean free path is comparable to $L_\parallel$).

We conclude this section with a note of caution on the use of Eqs. (39)–(41). Because our expressions for χ are still primitive, missing, among other things, details of the field-line geometry, we have not attempted to include in the derivation of the scaling equations the detailed geometrical factors retained by Barr [16]. Hence, while we would argue that the scaling dependencies are significant, the numerical values must be regarded as rough approximations. Another problem is that the parameter G is not a constant, but rather depends on the temperature and L_{Te}, and so should be self-consistently determined as the scaling laws are evaluated.

VII. Application to DIII-D and ITER

We evaluate the expressions derived in this paper for nominal DIII-D and ITER parameters. For DIII-D with a nominal set of paremeters typical of experimental operation, $T_e(s_d) = 17$ eV, $L_{Te} = 1.2$ cm, $Z_{eff} = 3$, $Z = 1.5$, $(1 + \gamma_{si}) = 1.5$ and $\delta = 1$, we find that $K_T \approx 1.7$ and hence, from Fig. 4 [or equivalently, from the solution of Eqs. (24) and (25)] that $G \approx 1.3$. (For $Z = 1$ we would have $K_T \cong 1$ and $G \approx 2$). Therefore Eq. (23) predicts $\chi_{ml} \approx 1$ m^2/sec. Note that finite $k_\parallel$ effects are significant, lowering the mixing-length diffusivity by a factor of almost two. If we consider a broader range of parameters $T_e(s_d) \sim 10 - 25$ eV, $L_{Te} \sim 1 - 2$ cm, we find $\chi_{ml} \cong 0.3 - 3$ m^2/sec. For our nominal set, we also find that at the maximum growth rate, $\mathrm{Re}\,\Omega/2\pi \sim 40$ kHz, and, according to the remarks made following Eq. (26), we expect a broad spectrum extending largely downward from there, roughly in agreement with experimental observations[17]. If we evaluate Eq. (30) for DIII with our nominal parameters (except L_{Te}) and $f_p \equiv \langle nT_e \rangle / nT_e(s_d) = 2$, $F_r = 0.35$, $\gamma_{se} = f_x = 0$, we obtain we obtain $L_{Te} \cong 1.1$ cm, again in approximate accord

with experiment. Finally, if we estimate T_e, L_{Te}, and λ_t in terms of input power from Eqs. (40)-(41), we obtain $T_{e0} \approx 84$ eV and $L_T \approx 0.8$ cm, and $\lambda_t \approx 6.3$ for $P = 2$ MW. The other parameters involved are $R = 1.6$ m, $L \approx 40$ m, $L_{pol} \approx 8$ m, $B/B_p \approx 6$, $n_{19} = 2$, and $\langle B_p \rangle / B_{p0} = 0.5$, and $B = 2$ T.

In applying the results to ITER, there is uncertainty in the choice of G. For ITER parameters, K_T is large enough that several $k_\parallel$ harmonics have appreciable growth rates, and, for each, $\mathrm{Im}\,\hat{\Omega}_m / Re\hat{\Omega}_m$ is small ($\sim 0.1 - 0.2$). In the absence of a detailed nonlinear theory, it is unclear how to best estimate the transport. One can construct arguments for estimates ranging from summing γ/k^2 over parallel harmonics to taking the largest single γ/k^2 and reducing that by $(\gamma/\mathrm{Re}\,\Omega)^{1/2}$. If we adapt the first (higher-χ) estimate and apply the scalings Eqs. (40)–(41) to parameters representative of the ITER Conceptual Design Activity (CDA) [4], we obtain $L_{Te} \approx 1.9$ cm, $T_{e0} \approx 145$ eV, and $\lambda_t \approx 1.05$ for $P = 175$ MW, $R = 6$ m, $B = 4.8$ T, $L \approx 130$,m, $L_{pol} \approx 14.5$ m, $B/B_p \approx 2.9$, $F_r \approx 0.47$, $n_{19} = 3$, $Z_{\mathrm{eff}} = 2$, $Z = 1.2$, and $\langle B_p \rangle / B_p = 0.32$. These parameters are consistent with $K_T \approx 5.4$ and hence, from solutions to Eq. (24), with $G \approx 4$, which is used to obtain the above results. For this K_T, three $k_\parallel$ harmonics (the $\theta = \pi/2$, $3\pi/2$ and $7\pi/2$ modes) contribute at an appreciable ($> 10\%$) level or greater; we keep these three in the sum to calculate G. Alternatively, the lower-χ estimate described above gives $G \approx 0.8$ and hence $L_{Te} \approx 1.2$ cm., $T_{e0} \approx 160$ eV, and $\lambda_t \approx 1.04$. The ITER CDA has a double-null divertor design. These calculations assume that essentially all of the power goes into the outboard SOL, and the calculation is for the width of that SOL. If we assume a more even split and assign 110 MW to the outer SOL, the scaling equations with $G = 4$ yield $L_T \approx 1.7$ cm, $T_{e0} \approx 102$ eV, and $\lambda_t \approx 1.25$. This illustrates that the SOL width is predicted to increase with increasing power, in contrast to the constant-χ model considered by Barr [16]. Note that L_{Te} for ITER is one to almost two times that for DIII-D. This conclusion is significantly more optimistic (less heat flux density on the divertor plates) than those obtained (*e.g.*, in Ref. 16) assuming a constant χ_e. Finally, we comment that, if we were to model a single-null ITER by doubling L and L_{pol} but keeping all other parameters the same, K_T would increase to about 8, increasing the relative role of higher-$k_\parallel$ harmonics.

VIII. Summary and Discussion

We have extended the theory of Berk, Ryutov and Tsidulko [1,2] and demonstrated that the instability they describe should be important in tokamak scrape-off layers. The extensions include an eigenmode equation derived from two-fluid theory which allows more careful calculation of finite $k_\parallel$ effects and explicitly displays the transition between the low-β electromagnetic and electrostatic regimes (at $k_\perp^2 c^2/\omega_{pe}^2 \approx 1$), addition of secondary electron emission and recycling, and an extended discussion of nonlinear effects.

The open-field-line region of a tokamak typically consists of two different regions: a thin scrape-off layer (SOL), energized by the heat escaping from the core plasma, and a more extended halo, fueled and powered by local sources. The electron-temperature-gradient-driven turbulence described in this paper can operate in both regions, although the drive is considerably higher in the thin SOL. The transport analysis described in Sec. V applies only to the SOL. In equilibrium, the electron energy end-loss rate exceeds that for ions (for $T_{ed} \gtrsim T_{id}$) because of the effect of the sheath potential, while both exceed the particle end-loss rate, because of the effect of recycling. Hence, apart from differences between the electron and ion thermal diffusivities and the particle diffusion coefficient (which cannot be resolved at the level of the present theory), we would expect $L_{Te} < L_{Ti} < L_n$, though not by large factors; roughly, $L_{Te}/L_{Ti} \approx \Lambda^{-1/2}$, and $L_{Ti}/L_n \sim (1-\gamma_r)^{1/2}$ if the recycling coefficient is treated as constant. If temperature dependence of the recycling coefficient is included, the density scale length is likely to be dominated by the scale length of the recycling coefficient, in which case we might expect $L_n \approx L_{Te}$. We furthermore see that the predicted L_{Te} values based on our transport analysis and using our derived diffusivities are comparable with those observed in experiments (around 1 cm for DIII-D [18]. The halo region is dominated by local sources; hence profile scale lengths cannot be determined without a more detailed description of these sources.

Based on the linear analysis, we expect that $\tilde{n}/n$, $\tilde{T}_e/T_e$, $\tilde{T}_i/T_i$ and $e\tilde{\phi}/T_e$ should be approximately in the ratio $1/L_n$ to $1/L_{Te}$ to $1/L_{Ti}$ to $\Omega/\omega_{eTd}^* L_{Te}$, respectively, and they should all be roughly in phase. In the core-energized scrape-off layer, we would expect to see $e\tilde{\phi}/T_e > \tilde{T}_e/T_e \gtrsim \tilde{n}/n > \tilde{T}_i/T_i$, where we have assumed temperature dependence to the recycling coefficient as in the preceding paragraph. In the halo, the inequalities could

shift because of the effect of local sources. Since, for example, in DIII-D, L_{Te} appears to be smaller than L_n in the SOL but larger than L_n in the halo [18], we would expect $\tilde{n}/n$ and $\tilde{T}_e/T_e$ to be oppositely ordered in the two regions.

An important implication of the theory is that it predicts larger scrape-off-layer widths than models based on extrapolation of present experimental data using a constant thermal diffusivity. This is primarily the result of the fact that our diffusivity has a significant scaling with the electron temperature at the sheath ($\propto T_{ed}^{3/2}$ in the flute limit). This parameter is considerably greater in a reactor than in current experiments, both because the average temperature in the SOL is higher and because the collisionality is lower (so that T_{e0}/T_{ed} is closer to 1). Finite-β, finite-$k_\parallel$ effects may also contribute to an increase in the diffusivity.

Based on the nonlinear consideration of an inverse cascade of wave energy, we expect a spectrum extending downward in wavenumber and frequency from the most unstable values, and a break in the shape of the spectrum around the most unstable frequency. For nominal DIII-D parameters this is at about 40 kHz, in rough accord with observations [17].

The theory as presented is incomplete in a number of respects. Because, at the most unstable wavelengths, $k_\perp L_{Te}$ is a significant fraction of unity for typical SOL parameters, the radially local approximation is marginal. An analysis of the radial differential equation would yield information about both the effect of equilibrium variations comparable to radial wavelengths within the SOL, and coupling to the closed-field-line region. Effects of parallel gradients in equilibrium quantities in the bulk of the field line are ignored, as are equilibrium current flows. While magnetic shear should not be as important in the open-field-line region as on closed field lines, one still has field-line fanning effects which introduce axial dependence to $k_\perp$ which can quantitatively affect the mode. Nonlinear effects are dealt with only at the most primitive level. Finally, the analytic work should be complemented by fluid and particle simulations. These will be addressed in future publications.

Acknowledgments

The encouragement of D. Duchs in applying the instability to tokamak scrape-off

layers is gratefully acknowledged. This work was performed in part under the auspices of the U.S. Department of Energy by The University of Texas, under Contract No. DE-FG05-80-ET-53088, by Lawrence Livermore National Laboratory under Contract No. W-7405-Eng-48, and by U.C. Berkeley under Grant No. DE-FG03-90-ER-54079.

Appendix

We derive here the maximum growth rates which follow from Eq. (24) for large K_T. We consider first the $\ell\pi/2$ modes. We observe that, for large K_T and nearly real $\theta(\hat{\Omega})$, where $\theta(\hat{\Omega}) \equiv k_\parallel L/2$ is the argument of the tangent function, T becomes small except when θ becomes close to $\ell\pi/2$ where ℓ is an odd integer. Hence there are roots of Eq. (24) with $\hat{\Omega} \sim \hat{k}$, and the growth rate will be maximized for $\hat{k}$ such that $k_\parallel \approx \ell\pi/2$. Hence we write $\hat{\Omega} = \hat{\Omega}_0 + \tilde{\Omega}$ with $\hat{\Omega}_0 = \hat{k}$, and expand the tangent about $\theta = \ell\pi/2$, writing $\tan\theta \approx [-\theta_{\hat{\Omega}}\tilde{\Omega}]^{-1}$, where $\theta_{\hat{\Omega}} \equiv \partial\theta/\partial\hat{\Omega}$. With these approximations we can solve Eq. (24) and maximize the growth rate over $\hat{k}$ to obtain

$$\tilde{\Omega}_{\ell m} \approx (-1+i)(\ell\pi/2)^{3/2} K_T^{-5/2} \frac{1}{[2+\delta]^{1/2}(1+\delta)^{1/4}} \qquad (A1)$$

and $\hat{k}_{\ell m} = \ell(\pi/2)K_T^{-1}[1/(1+\delta)]^{1/2}$.

Note, however, that higher ℓ are more unstable (although the mixing-length diffusivity decreases with ℓ as $\ell^{-1/2}$). In fact, for any K_T, when $\ell \sim K_T$, then the perturbation expansion, which was based on treating $\mathrm{Im}\,\theta \ll 1$, fails. For $\ell \sim K_T$, we note that $\mathrm{Im}\,\tilde{\Omega}_{\ell m} \sim K_T^{-1}$. We can look for shorter-parallel-wavelength solutions by making the opposite approximation, *i.e.* that $\mathrm{Im}\,\theta \gg 1$. In that limit we can approximate $\tan\theta \approx i[1-\exp(2i\theta)]$. Then we can split Eq. (25) into its real and imaginary components,

$$-\frac{\theta_i}{K_T^2} + 2\frac{\theta_r}{K_T^2}\sin(2\theta_r)\exp(-2\theta_i) - \frac{\hat{\Omega}_i}{\hat{k}^2} \cong 0 \qquad (A2)$$

$$\frac{\theta_r}{K_T^2} + \frac{\hat{\Omega}_r}{\hat{k}^2} - \frac{i}{\hat{k}} \cong 0 \quad , \qquad (A3)$$

respectively, where θ_r and θ_i are the real and imaginary parts of θ, and similarly for $\hat{\Omega}$. If we now restrict attention to the case $\delta = 0$, then $\theta = K_T\hat{\Omega}$, and we can explicitly solve Eq. (A3) to obtain $\hat{\Omega}_r \cong K_T\hat{k}/(K_t + \hat{k}^2)$. We note from Eq. (A2) that $\hat{\Omega}_i$ increases with $\hat{\Omega}_r$, and, from the expression we have just obtained, $\hat{\Omega}_r$ is maximized as a function of $\hat{k}$ when $\hat{k} = K_T^{1/2}$, in which case $\hat{\Omega}_r \cong K_T^{1/2}/2$. This is large for large K_T. Hence, in the vicinity of the maximum (of both real and imaginary parts of $\hat{\Omega}$), and when the sine in Eq. (A2) is positive and not near zero, we can write

$$K_T\hat{\Omega}_i \approx (1/2)\left(\ln(K_T\hat{\Omega}_r) - \ln\ln(K_T\hat{\Omega}_r) + \ln[\sin(2K_T\hat{\Omega}_r)]\right) \quad . \qquad (A4)$$

The maximum growth rate is thus $\mathrm{Im}\,\hat{\Omega}_m \approx (3/4)K_T^{-1}\ln K_T$. Note that this maximum growth rate is in fact a decreasing function K_T, while the corresponding wavenumber is becoming large; hence the mixing-length diffusivity is decreasing as $\ln K_T/K_T^2$.

Finally, we consider the "high-wavenumber" modes for which $\mathrm{Re}\,\theta \sim \mathrm{Im}\,\theta \sim 1$. For these modes, $\hat{k} \sim K_T^2$, and $\hat{\Omega} \sim K_T^{-1}$ for $\delta = 0$ and $\hat{\Omega} \sim \delta^{-1}K_T^{-3}$ for $\delta \neq 0$. Hence the second term in Eq. (24) is smaller than the first or third by $\mathcal{O}(K_T^{-3})$ and $\delta^{-1}K_T^{-5}$ for $\delta = 0$ and $\delta \neq 0$, respectively. Once the second term is dropped, K_T can be scaled out of Eq. (24) by introducing $\kappa = K_T^{-2}\hat{k}$. Hence we obtain

$$\theta^2 \tan\theta - i/\kappa = 0 \quad . \tag{A5}$$

There is a series of roots corresponding to different branches of $\tan^{-1}$. For $\delta = 0$, we have $\theta = K_T\hat{\Omega}$; thus maximizing the growth rate is equivalent to maximizing $\mathrm{Im}\,\theta$. the first three such modes are, after maximizing the growth rates with respect to κ, $\theta_m \cong (1.042 + 0.6013\,i)$ at $\kappa_m = 0.6616$, $\theta_m \cong (3.9893 + 1.0287\,i)$ at $\kappa_m = 0.2353$, and $\theta_m \cong (7.1032 + 1.227\,i)$ at $\kappa_m = 0.1371$. The growth rate appears to be a weakly increasing function of mode number, a trend continued for at least the next two modes beyond those just given.

For $\delta \neq 0$, $\theta(\hat{\Omega})$ is given by the right-hand side of Eq. (25); for large K_T (formally, $\delta K_T^{5/2} \gg 1$), we find that $\hat{\Omega} \cong \theta^2/\delta K_T^3\kappa$. Hence, in this limit, $\mathrm{Im}\,\Omega$ is maximized by maximizing $\mathrm{Re}\,(\theta)\mathrm{Im}\,(\theta)/\kappa$. We find that the growth rate is maximized for $\kappa \to 0$, in which limit $\theta \to (\pi/2)(1 + i\kappa)$. Note that we are not free to take the limit $\kappa \to 0$ for finite K_T as this invalidates the neglect of the second term in Eq. (24). Hence we cannot infer, from this analysis, $\hat{k}_m$ and $\mathrm{Re}\,\hat{\Omega}_m$. The limiting expression for $\hat{\gamma}$ is well-defined, and is $\hat{\gamma}_m \cong \pi^2/2\delta K_T^3$. We immediately deduce that this root is distinct from the first of the $\ell\pi/2$ modes, as it has a different growth rate. We have identified both $\pi/2$ modes from numerical solutions of Eq. (24), and observe that the "high-wavenumber" mode in fact has higher wavenumber $\hat{k}_m$. (See, for example, Fig. 4.) The next two modes have maxima which distinguishes them from the $\ell\pi/2$ modes; maximum growth occurs for $\theta = 4.549 + 0.7247\,i$, $\kappa = 0.1385$, and $\theta = 7.563 + 1.044\,i$, $\kappa = 0.1066$, respectively. The corresponding frequencies and wavenumbers $\hat{\Omega}_m$ and $\hat{k}_m$ are $\hat{\Omega}_m \cong (145.6{+}47.61i)/\delta^{-1}K_T^{-3}$

at $\hat{k}_m = 0.1385 K_T^2$, and $\hat{\Omega}_m \cong (526.4 + 198.1\, i)/\delta^{-1} K_T^{-3}$ at $\hat{k}_m = 0.1066 K_T^2$, respectively.

REFERENCES

[1] BERK, H.L., RYUTOV, D.D. and TSIDULKO, YU., JETP Lett. **52**(1990) 674.

[2] BERK, H.L., RYUTOV, D.D. and TSIDULKO, YU., Phys. Fluids B **3**(1991) 1346.

[3] KADOMTSEV, B.B., in *Proc. 7th Conf. on Phenomena in Ionized Gases*, (Belgrade, 1965, Ed. B. Perovic and D. Tocsic) Grad Jevinska Kniga, Belgrade, Yugoslavia (1966), Vol. 2, p. 610.

[4] POST, D.E., *et al.*, ITER Physics, Iter Documentation Series No. 21, [International Atomic Energy Agency, Vienna, 1991].

[5] NEDOSPASOV, A.V., Fiz. Plazmy **15**(1989) 1139 [Sov. J. Plasma Phys. **15**(1989) 659].

[6] GARBET, X., LAURENT, L., ROUBIN, J.-P. and SAMAIN, A., Nucl. Fusion **31**(1991) 967.

[7] KUNKEL, W., and GUILLORY, J., in *Proc. 7th Conf. on Phenomena in Ionized Gases*, (Belgrade, 1965, Ed. B. Perovic and D. Tocsic) Grad Jevinska Kniga, Belgrade, Yugoslavia (1966)., Vol. 2, p. 702.

[8] ALLEN, S.L., RENSINK, M.E., HILL, D.N., *et al.*, J. Nucl. Mater. **162**(1980) 80; BUCHENAUER, D.,SHU, W.L., HILL, D.N., *et al.*, J. Nucl. Mater. **176**(1990) 528; HILL, D.N., RENSINK, M.E., FUTCH, A., *et al.*, J. Nucl. Mater. **176**(1990) 53.

[9] BRAGINSKII, S.I., in *Reviews of Plasma Physics*, Vol. 1 (Consultant's Bureau, New York, 1965), p. 105.

[10] BERK, H.L., RYUTOV, D.D., STUPAKOV, G.V., and TSIDULKO, YU.A., in *Plasma Physics and Controlled Nuclear Fusion Research 1990*, Washington, D.C., (IAEA, Vienna, 1991), Vol. 2, p. 289.

[11] HINTON, F.L. and HORTON, C.W., Jr., Phys. Fluids **14**(1971) 116.

[12] TSAI, S., PERKINS, F.W., and STIX, T.H., Phys. Fluids **13**(1970) 2108.

[13] SELF, S.A. and EWALD, H.N., Phys. Fluids **9**(1966) 2486.

[14] BOERNER, E., COHEN, R.H., NEWCOMB, W.A., and CROTINGER, J.A., to be submitted to Phys. Fluids.

[15] WAKATANI, M. and HASEGAWA, A. Phys. Fluids **27**(1984) 611.

[16] BARR, W., Fusion Technology **19**(1991) 498.

[17] MOYER, R.A., WATKINS, J.G., BURRELL, K., CONN, R.W., DOERNER, R., HILL, D., LEHMER, R., MAHDAVI, M.A., SCHMITZ, L., and TYNAN, G., Bull. Am. Phys. Soc. **36**(1991) 2472.

[18] WATKINS, J.G., MOYER, R.A., BUCHENAUER, D., DOERNER, R., HILL, D., LEHMER, R., MAHDAVI, M.A., and SCHMITZ, L., Bull. Am. Phys. Soc. **36**(1991) 2472.

Figure Captions

FIG. 1. Normalized growth rate $\hat{\gamma}$ and real frequency $\mathrm{Re}\,\hat{\Omega}$ vs. normalized wavenumber $\hat{k}$ for various values of δ.

FIG. 2. Variation with δ of normalized frequency $\hat{\Omega}_m$, wavenumber $\hat{k}_m$, and mixing-length diffusivity $\hat{\Omega}_m/\hat{k}_m^2$ at the maximum growth rate.

FIG. 3. Finite-$k_\parallel$ effects for $\delta = 0$: (a) and (b) are fundamental $k_\parallel$ root; (c) and (d) are for first harmonic. (a) and (c) show $\hat{\Omega}_m$ vs. K_T; (b) and (d) show $\hat{k}_m$ and $\hat{\gamma}_m/\hat{k}_m^2$ vs. K_T.

FIG. 4. Finite-$k_\parallel$ effects for $\delta = 1$: (a) and (b) are fundamental $k_\parallel$ root; (c) and (d) are for first harmonic. (a) and (c) show $\hat{\Omega}_m$ vs. K_T; (b) and (d) show $\hat{k}_m$ and $\hat{\gamma}_m/\hat{k}_m^2$ vs. K_T.

FIG. 5. Solutions of model transport equations (31) and (32). (a) is T_i/T_{i0}; (b) is n/n_0; (c) is T_e/T_{e0}; (d) is analytic solution T_e/T_{e0} from Eq. (34).

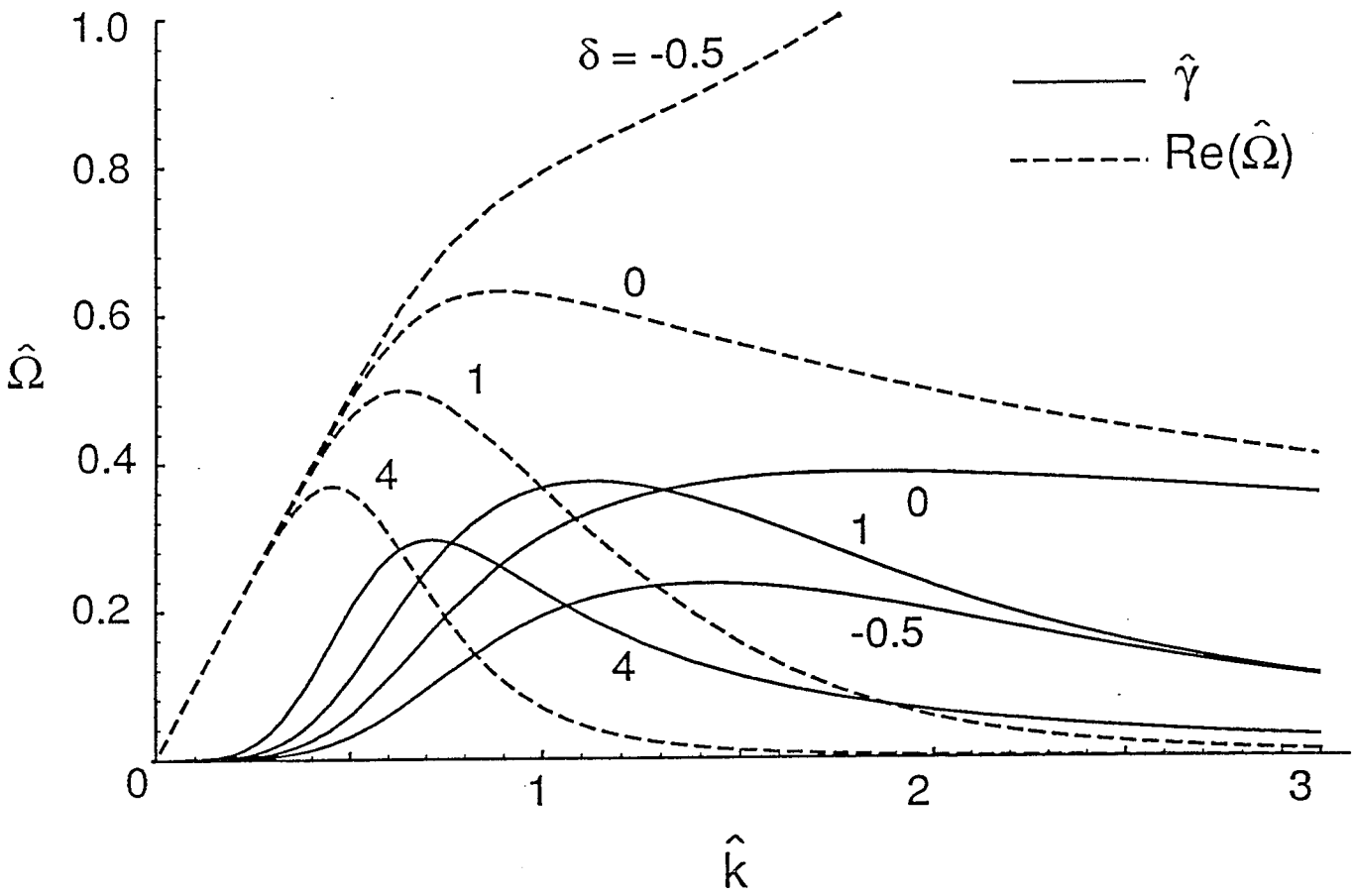
1.0
0.8
0.6
0.4
0.2
0
$\hat{\Omega}$
$\delta = -0.5$
$\hat{\gamma}$
$\mathrm{Re}(\hat{\Omega})$
0
1
4
0
1
-0.5
4
0
1
2
3
$\hat{k}$

Fig. 1

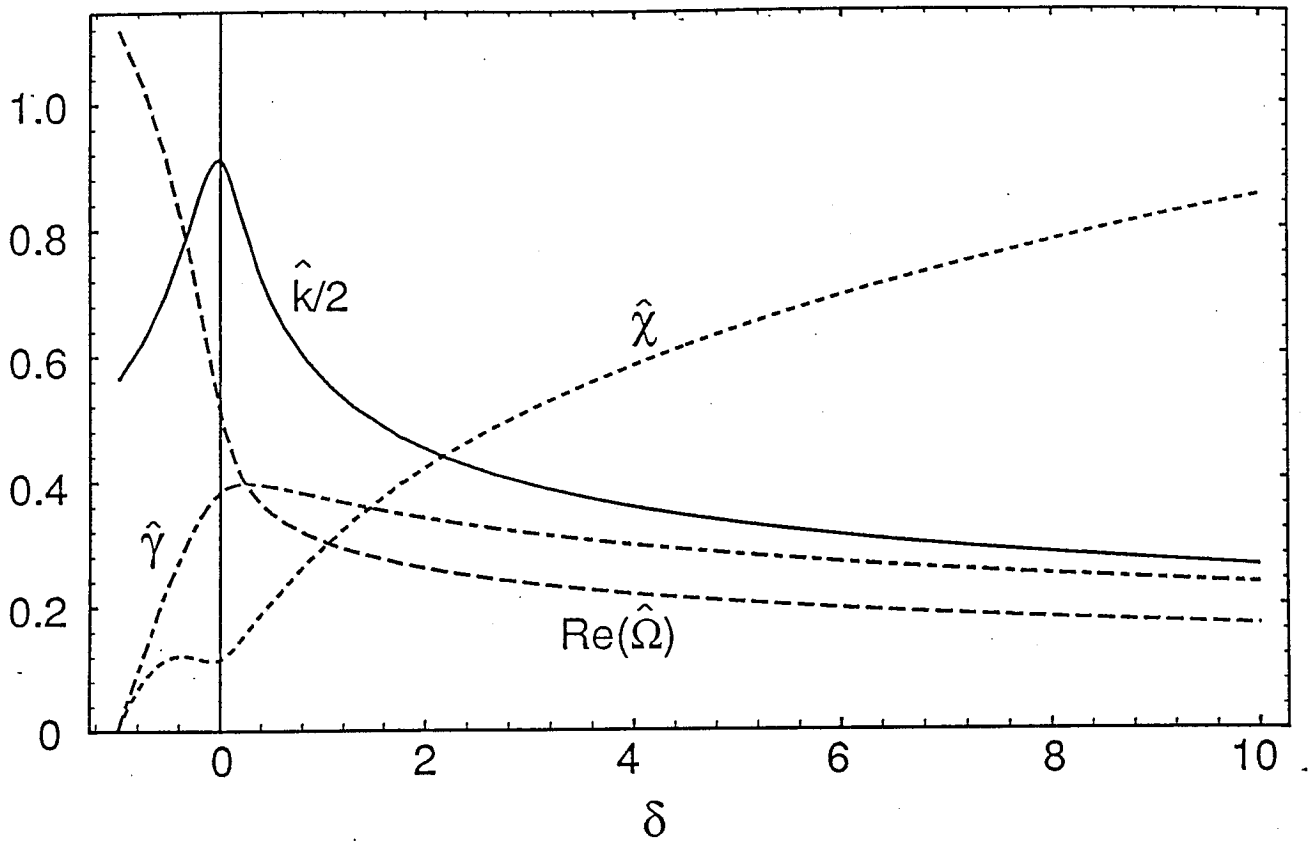

Fig. 2

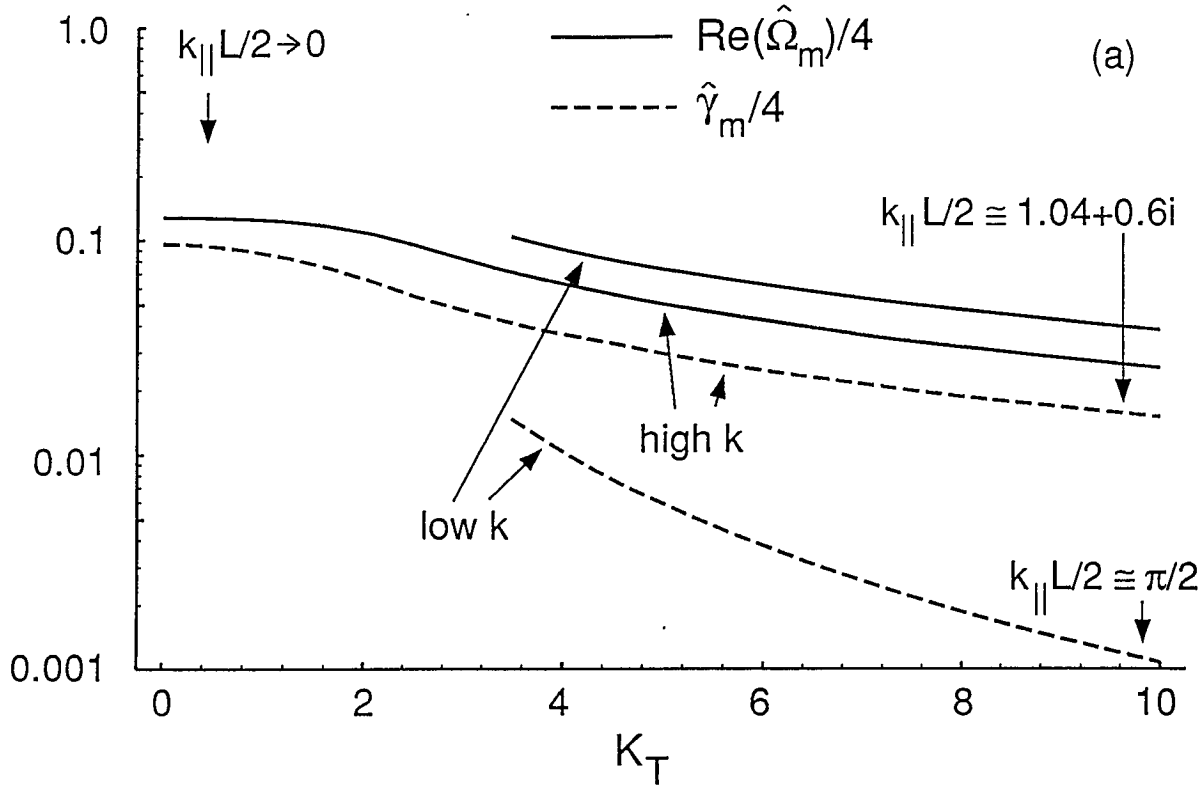
1.0
0.1
0.01
0.001
$k_{||}L/2 \to 0$
$\mathrm{Re}(\hat{\Omega}_m)/4$
$\hat{\gamma}_m/4$
(a)
$k_{||}L/2 \cong 1.04+0.6i$
high k
low k
$k_{||}L/2 \cong \pi/2$
0
2
4
6
8
10
K_T

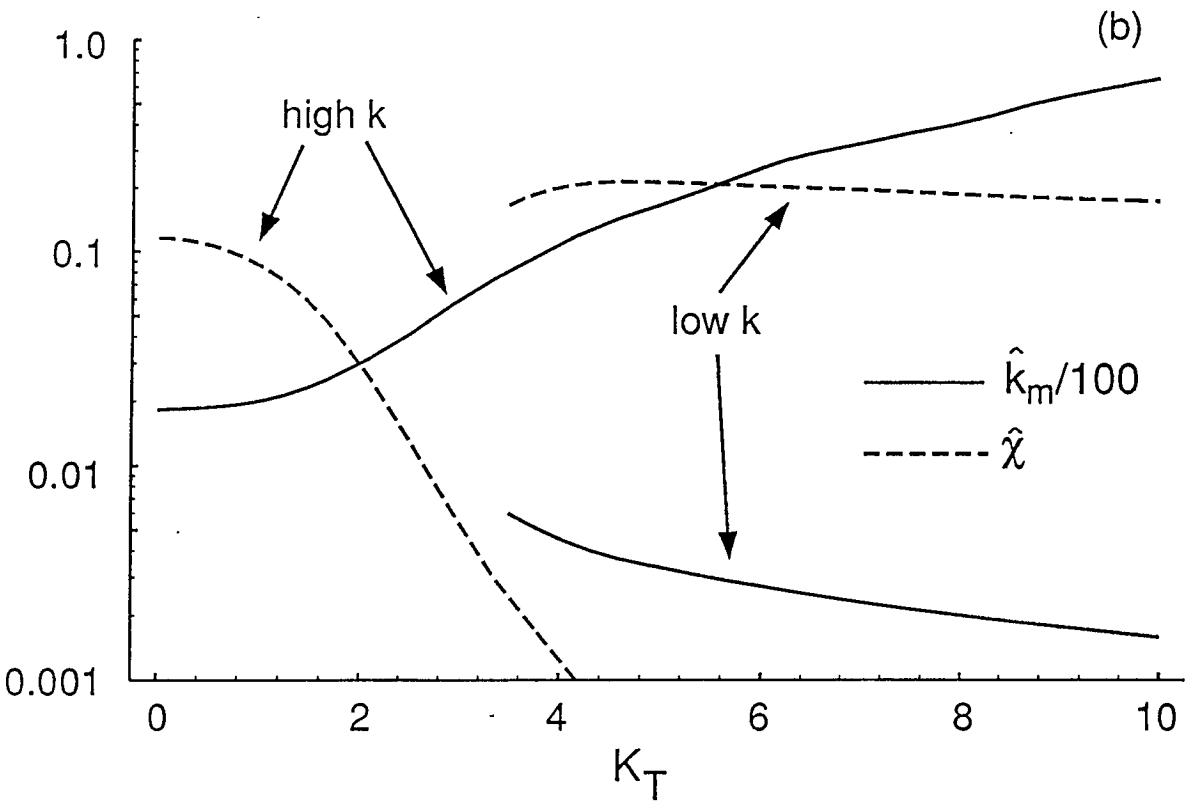
(b)
1.0
0.1
0.01
0.001
high k
low k
$\hat{k}_m/100$
$\hat{\chi}$
0
2
4
6
8
10
K_T

Fig. 3

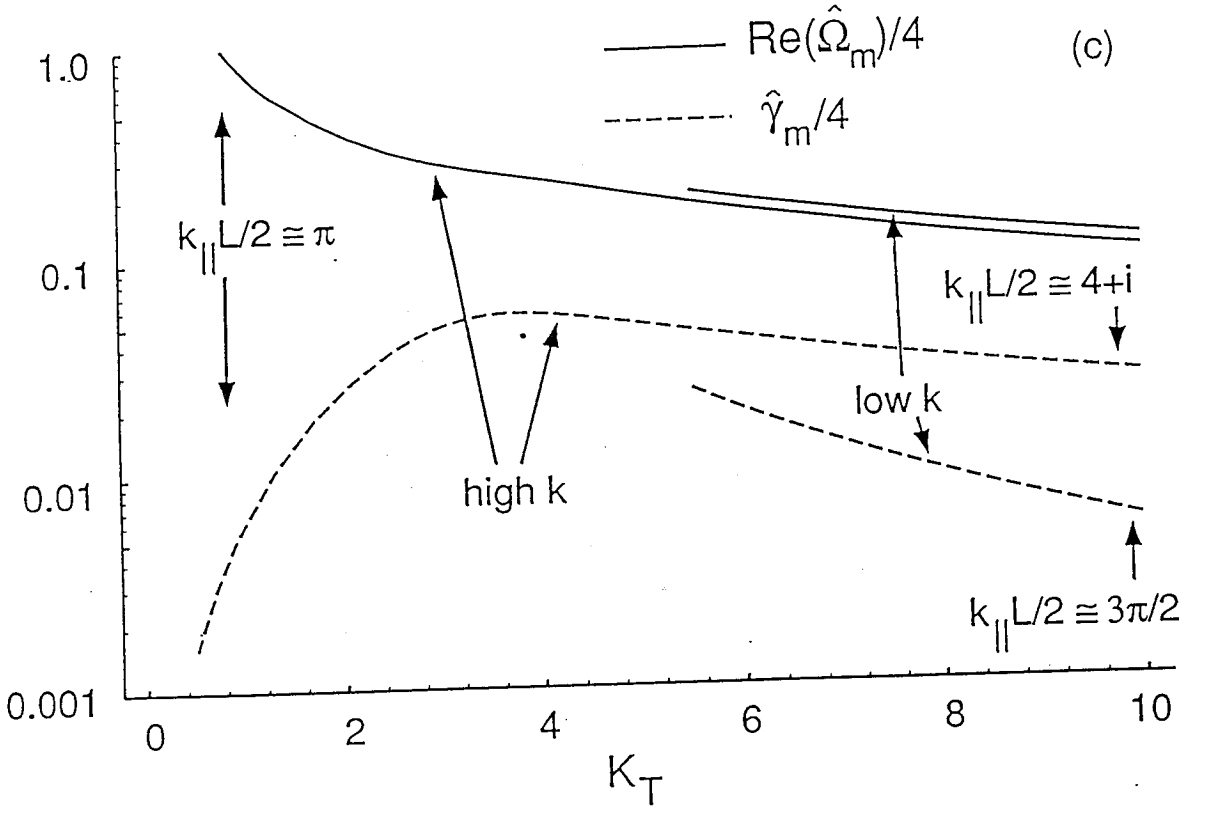
Re($\hat{\Omega}_m$)/4
(c)
$\hat{\gamma}_m$/4
1.0
0.1
0.01
0.001
$k_{||}L/2 \cong \pi$
$k_{||}L/2 \cong 4+i$
low k
high k
$k_{||}L/2 \cong 3\pi/2$
0
2
4
6
8
10
K_T

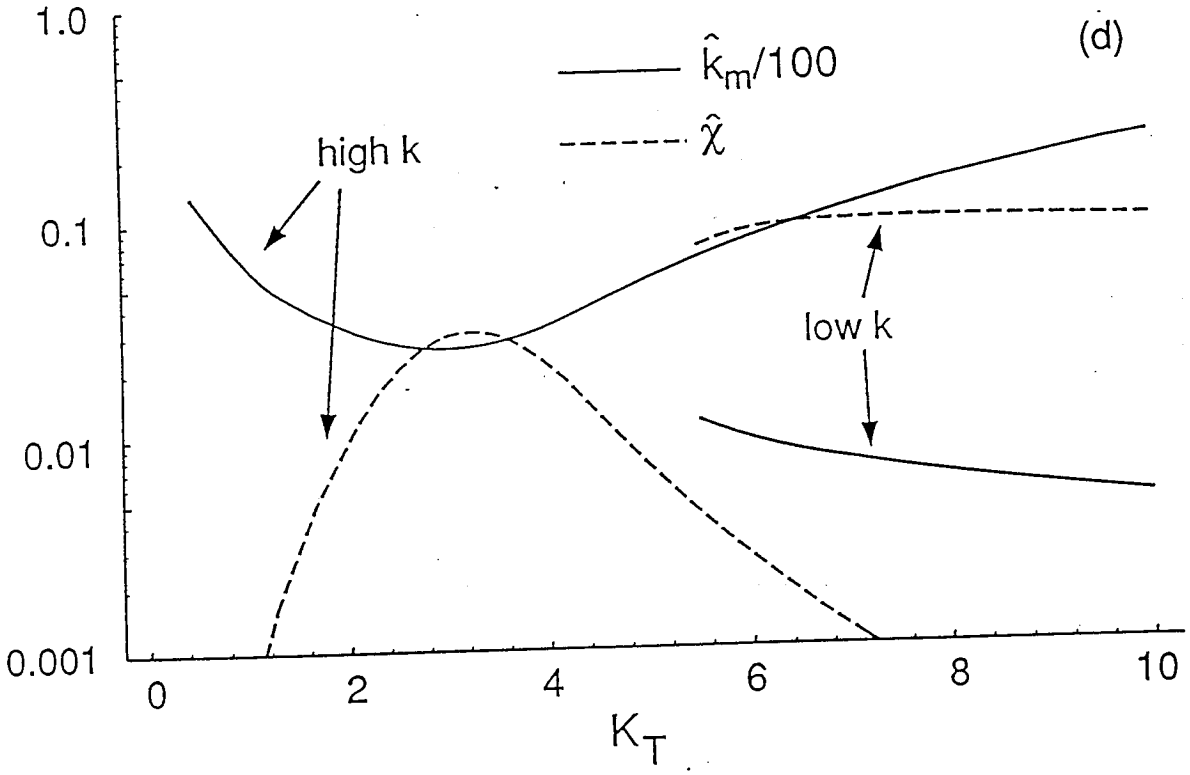
$\hat{k}_m$/100
(d)
$\hat{\chi}$
high k
1.0
0.1
0.01
0.001
low k
0
2
4
6
8
10
K_T

Fig. 3

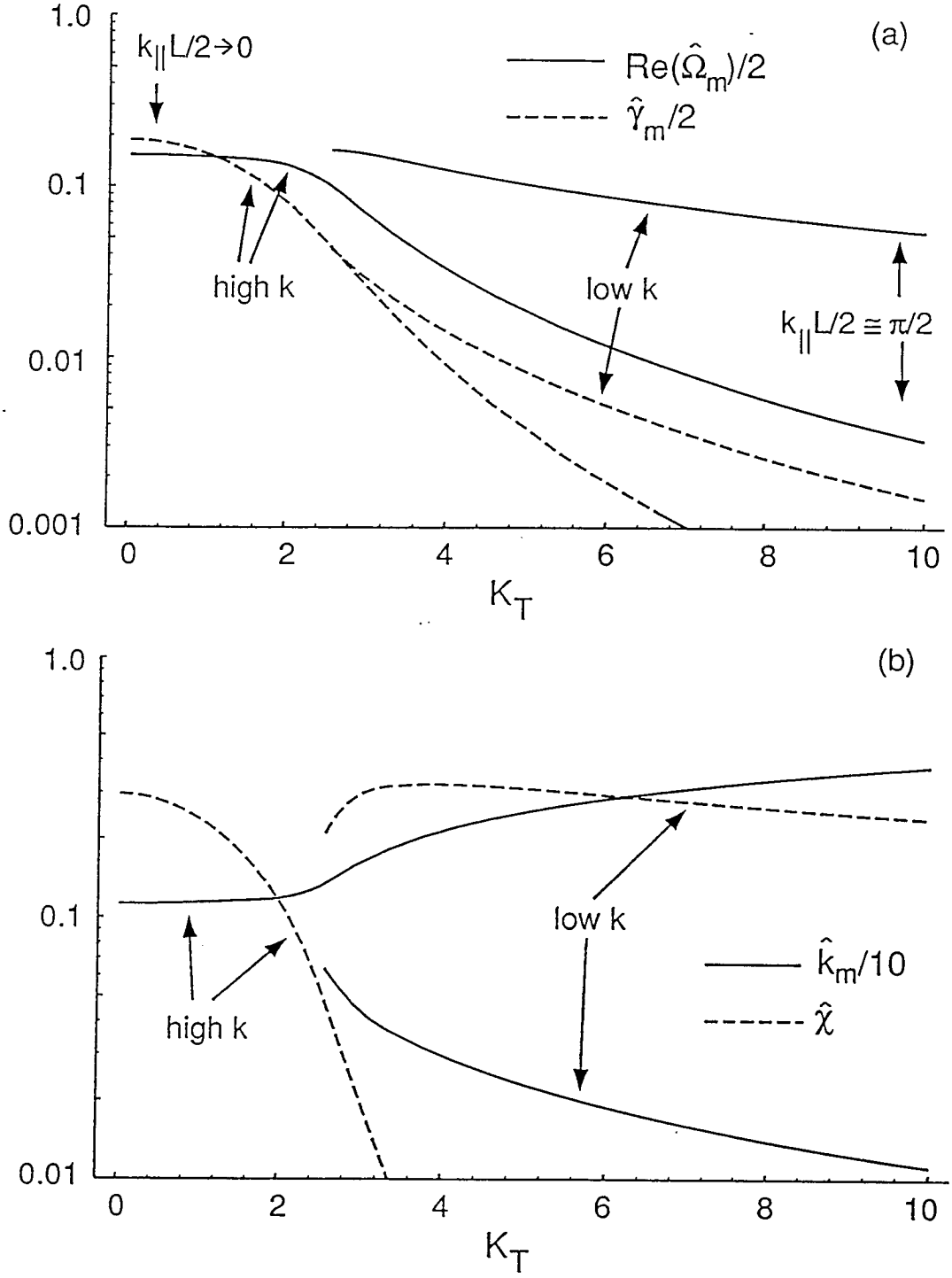
(a)
1.0
0.1
0.01
0.001
$k_{||}L/2 \to 0$
$\mathrm{Re}(\hat{\Omega}_m)/2$
$\hat{\gamma}_m/2$
high k
low k
$k_{||}L/2 \cong \pi/2$
0
2
4
6
8
10
K_T
(b)
1.0
0.1
0.01
low k
high k
$\hat{k}_m/10$
$\hat{\chi}$
0
2
4
6
8
10
K_T

Fig. 4

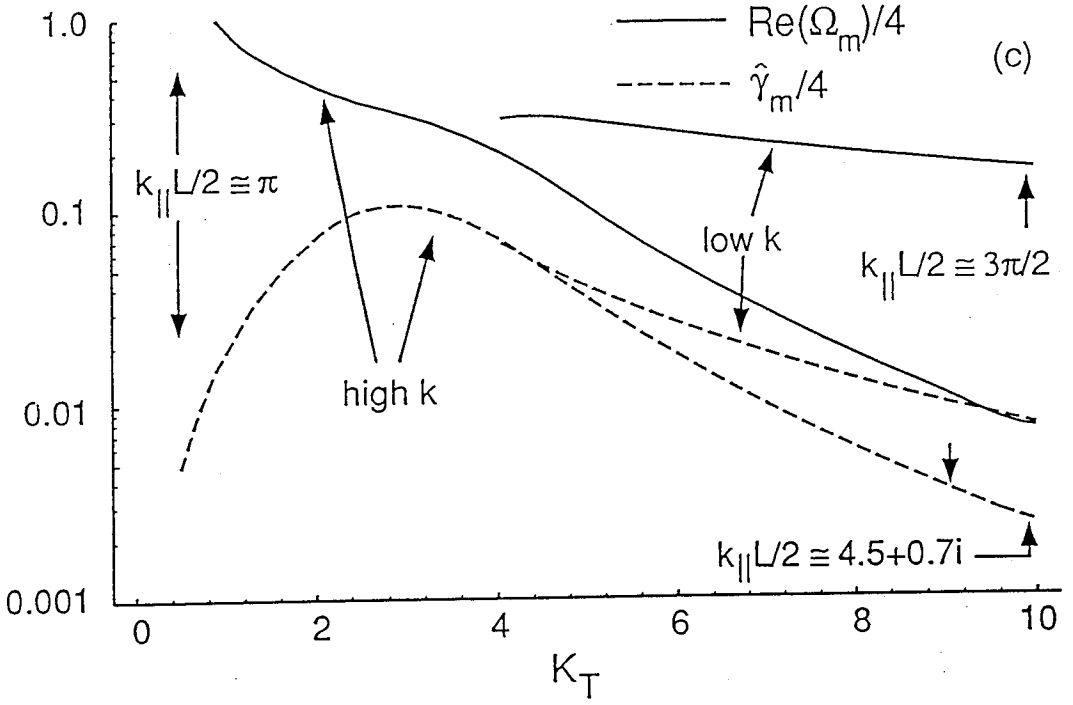
1.0
0.1
0.01
0.001
0
2
4
6
8
10
K_T
$\mathrm{Re}(\hat{\Omega}_m)/4$
$\hat{\gamma}_m/4$
(c)
$k_{||}L/2 \cong \pi$
high k
low k
$k_{||}L/2 \cong 3\pi/2$
$k_{||}L/2 \cong 4.5+0.7i$

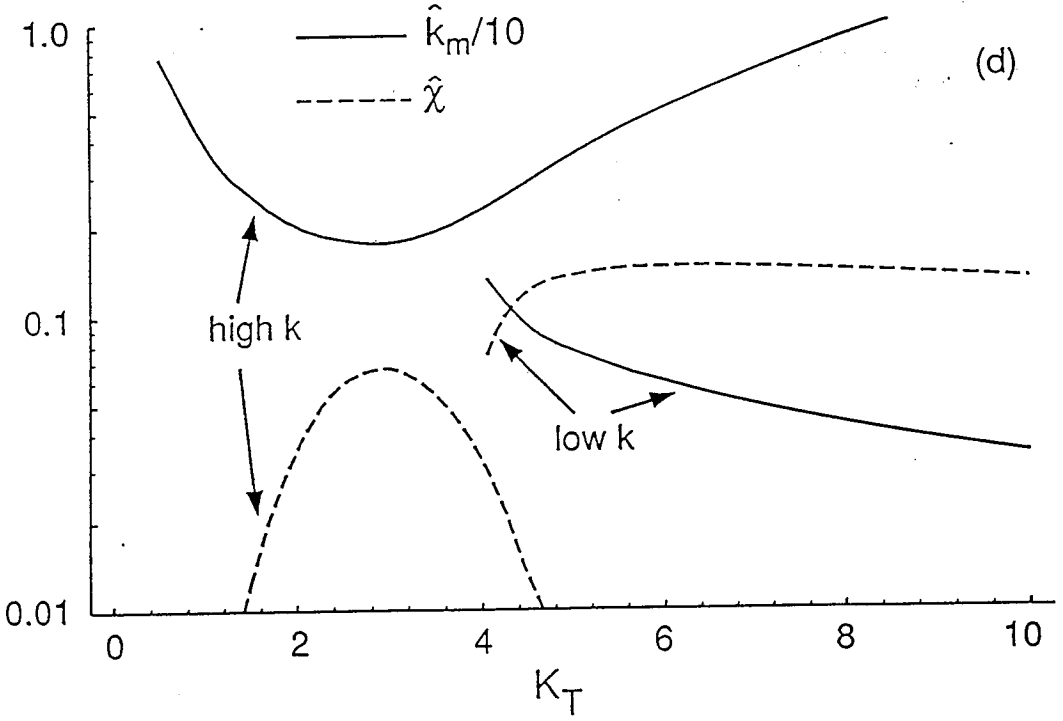
1.0
0.1
0.01
0
2
4
6
8
10
K_T
$\hat{k}_m/10$
$\hat{\chi}$
(d)
high k
low k

Fig. 4

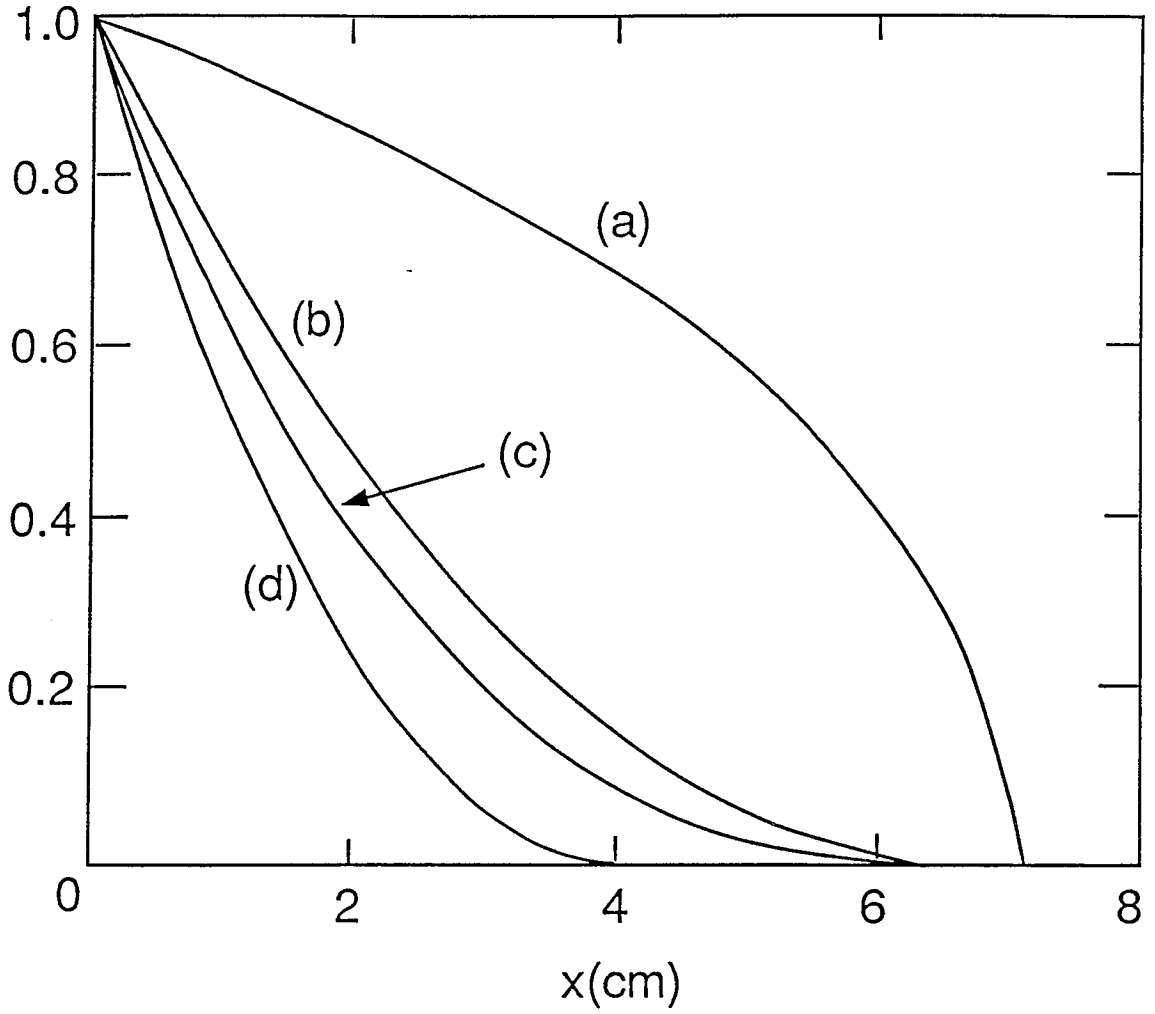

Fig. 5